nature portfolio

Peer Review File

Bidirectional electron donation in Cu1–Ti pairs on TiOx for efficient nitric oxide electroreduction

Corresponding Author: Professor Yancai Yao

This file contains all reviewer reports in order by version, followed by all author rebuttals in order by version.

Version 0:

Reviewer comments:

Reviewer #1

(Remarks to the Author)
This work presents an interesting study on heteronuclear dual-atom catalysts for NORR. However, I recommend rejection due to several significant concerns.
First, the proposed mechanism relies heavily on computational models and indirect spectroscopic evidence. Direct experimental verification of the side-on Ti–N=O–Cu adsorption geometry under operating conditions is lacking. The in situ ATR-IRAS signals are insufficient to unambiguously assign this configuration.
Second, the catalyst synthesis is inadequately controlled. The formation of Cu–Ti pairs is inferred from EXAFS, but the possibility of small Cu clusters or oxides, especially after long-term testing, is not rigorously excluded. The post-stability characterization (XRD, XPS) is not convincing enough to confirm structural integrity.
Finally, the work does not sufficiently address selectivity. While NH_3 yield is high, potential by-products (e.g., N_2O, N_2, hydroxylamine) are not quantified or discussed. This omission weakens the practical relevance of the reported Faradaic efficiency.

Reviewer #2

(Remarks to the Author)
In this manuscript, the authors break away from the traditional single-site activation model of nitrogen oxide reduction reaction (NORR) and propose a design strategy for heteronuclear dual-sites cooperative catalysis. By leveraging the complementary affinities of Cu and Ti atoms toward O and N, they achieve a conformational shift of NO molecules from “end-on adsorption” to “side-on adsorption”, which facilitates the efficient activation of polar NO molecules. This work emphasizes the significance of atomic-level design in creating asymmetric active sites capable of efficiently activating and converting polar molecules to high-value products. Overall, the paper is well-written, with a logical flow and clearly presented results. Therefore, I believe this manuscript is highly suitable for publication on Nature Communications after minor revisions.
1. Given that NO can be oxidized to nitrate ions (NO3–) at the anode, which is then electro-reduced to ammonia at the cathode, a comparative analysis of the energy efficiency between the direct NO electro-reduction pathway and the indirect “NO→ NO3– → NH3” pathway should be included.
2. Since NORR typically yields multiple products (e.g., hydrazine and hydroxylamine), the authors should specify whether other byproducts were detected during testing. If so, corresponding characterization data and quantitative results must be provided.
3. The supplementary information should detail the calculation methodology for the “ECSA-normalized activity,” along with a corresponding figure, to enable direct comparison with prior studies.
4. Aberration-corrected SEM analysis of post-reaction catalyst structure is necessary to verify the retention of the Cu single-atom configuration.
5. Thermodynamic data (ΔE, ΔEZPE, and ΔS) should be included within the supplementary information to facilitate reproduction of theoretical results. In addition, in the supplementary XPS spectra, orbital symbols (e.g., 2p, 3d) should be presented in italics. To ensure accuracy, the authors should also meticulously review all figure and table information.

Reviewer #3

(Remarks to the Author)
In this manuscript, Zhang et al. report the fabrication of Cu1-Ti catalytic pairs on commercial titanium felt. This design is specifically tailored for the electrocatalytic reduction of NO to NH3. They discovered that unlike the end-on adsorption mechanism of NO on symmetric Ti-Ti pairs, the asymmetric Cu1-Ti pairs enable a novel side-on bidentate adsorption pathway. This adsorption behavior activates both ends of the N=O bond simultaneously, thereby promoting efficient activation of NO molecules and ultimately achieving high selectivity and yield in ammonia production.
The authors have systematically integrated experimental characterization, in situ spectroscopic analysis, and DFT calculations to elucidate the heteronuclear bidentate synergistic catalytic mechanism underlying the observed performance. On this basis, I recommend the publication of this manuscript in Nature Communications following appropriate revisions. Specific comments for revision are provided below.
1. Why was Cu chosen to form the Cu1-Ti pairs catalytic system? Are Fe1-Ti pairs, Co1-Ti pairs, or Ni1-Ti pairs feasible? Please provide corresponding explanations.
2. The specific contribution of the Cu-O-Ti shell in the FT-EXAFS R space needs to be determined to more clearly elucidate the Cu-O-Ti coordination relationship.
3. What is the Cu-Ti distance in Cu1-Ti pairs? From a theoretical perspective, how does this distance influence the adsorption configuration?
4. In poisoning experiments, the SCN^- poisoning test involves adding SCN^- directly to the electrolyte, while the S2- poisoning test employs an electrode immersion and rinsing procedure. What are the considerations behind these different approaches?
5. Hydroxylamine can serve both as an intermediate and as the final product of NORR. Distinct hydroxylamine signals appear in the infrared spectrum. Please indicate whether the product contains hydroxylamine or other non-ammonia substances.
6. Certain figures appear to be mislabeled or incorrectly captioned. The authors should verify that all figure labels and legends accurately correspond to the data presented.

Reviewer #4

(Remarks to the Author)
In this manuscript, the authors ingeniously designed a bimetallic site catalyst with a Cu-O-Ti structure, utilizing the synergistic effect of Cu and Ti to promote the electrochemical reduction of NO. The highest Faraday efficiency reached 93.7%, which is superior to the currently reported catalysts for the same reaction. At the same time, the d-π* coupling brought about by the bimetallic sites further promotes the transfer of electrons. Overall, the content of the article is rich and the structure is clear. However, the presentation of some experimental evidence is not sufficient, and there are some confusing parts. Additionally, regarding certain evidence chains, we have some concerns and would suggest that the authors revisit and potentially revise these sections to strengthen their argument.
1. The bimetallic site catalyst designed by the authors achieved a very high Faraday efficiency and electrocatalytic ammonia synthesis performance, but the research on control experiments and by-products was too weak. For instance, are there any relevant data directly proving the electrocatalytic ammonia synthesis performance of structures such as Cu-O-Cu? Additionally, for the reaction using NO as the raw material, are there any other N-N bonded products, such as N2, in the products?
2. Although HAADF-STEM and EXAFS data support the single-atom dispersion of Cu, the precise coordination structure and formation ratio of the Cu1-Ti heteronuclear bidentate pair have not yet been confirmed. The fitting path of the Cu-Ti scattering peak at 2.58 Å in EXAFS is not unique, and no synchrotron radiation data of the Ti K-edge is provided to verify the change in the coordination environment of Ti. Considering that there are various defect sites on the TiO2 surface, the current data cannot rule out the possibility that the Cu atoms are randomly distributed in different oxygen vacancies rather than forming a unified active pair. This structural uncertainty directly affects the credibility of the mechanism explanation.
3. Since the authors have already elaborated on the practical application scenarios of exhaust gas treatment in the background section, in the article, evidence should be used to support the corresponding viewpoints. We do not deny the excellent performance of the catalyst designed by the authors. However, the raw material used is a mixture of 20% NO and 80% Ar. The proportion of NO in this mixture is too high. Could the authors consider conducting relevant experiments in an environment with a low concentration of NO to further highlight the key points of the article? Especially when comparing the content of this article with the currently reported catalysts, we can see obvious performance differences under more demanding conditions. However, the current data fails to highlight the advantages of the bimetallic catalyst.
4. The improvements made in the manuscript regarding the activation mechanism of N=O based on the orbital theory are extremely fascinating. However, the rigor of some of the data may need to be further improved. For instance, in Fig 3e, the assignment of *NO (side-on) is rather arbitrary and lacks rigorous validation such as isotope labeling. This significantly undermines the theoretical explanations for "side-on adsorption" and "end-on adsorption". In addition, regarding the tests of the experimental results, we suggest that the authors should carefully consider the interference of K^+ ions in the electrolyte, surface hydroxyl groups, or other nitrogen-containing species.
5. The authors should carefully review all the details in the text. Some of the errors are quite detrimental to the readers' reading and comprehension. For example, the expression of uniformly occupied oxygen vacancies (Ovs and OVs); Regarding the correspondence of each figure in Fig 3 with the content of the article, as well as the explanation of the specific meaning of the symbol "|e|" that appears in the article and the relevant literature references.
6. The title of this manuscript was: “Bidirectional electron donation in heteronuclear catalytic pairs for efficient nitric oxide electroreduction to ammonia”. We think the title is too broad and overstated, implying that similar all catalysts are suitable without any specificity.

Reviewer #5

(Remarks to the Author)
This work reports a heteronuclear Cu1–Ti dual-atom catalyst for efficient electrocatalytic NO reduction to NH_3, leveraging complementary N/O affinities of Ti/Cu to achieve side-on adsorption and bidirectional electron transfer. The integration of experimental characterizations (e.g., in situ ATR-IRAS, DEMS) and DFT calculations is rigorous, and the catalyst exhibits impressive FE (93.7%) and NH_3 yield. Overall, I recommend its publication after minor revisions. Some specific comments are provided as follows.

1. The formation mechanism of Cu1-Ti pairs mentions oxygen vacancies (OVs) but lacks atomic-level details on how Cu precisely embeds into Ti–Ov–Ti motifs. Please supplement structural evolution evidence (e.g., ex situ XAFS at different annealing stages).
2. In Fig. 2f, comparisons with reported catalysts do not specify whether test conditions (e.g., NO concentration, electrolyte type) are consistent. Standardize parameters for fairer performance benchmarking.
3. DFT calculations use a TiO_2 surface model, but the specific crystal phase (anatase/rutile) is unspecified. Clarify this as it significantly affects adsorption energy and reaction pathways.
4. More recently reported literatures related to this work can be properly cited to make this paper state-of-the-art: Nat. Commun., 2025, 16, 8837. Adv. Mater., 2024, 36, 2402160.
5. Stability testing only includes 20 cycles. Provide long-term electrolysis data (e.g., 100 h) and post-reaction structural characterizations to verify resistance to agglomeration/deactivation.
6. The *NHO → *NH_2OH step in the reaction pathway lacks DFT-calculated free energy changes. Supplement this data to clarify its thermodynamic feasibility.
7. The introduction barely compares with the latest heteronuclear dual-atom NORR catalysts. Add key performance parameters (FE, yield) of recent works to highlight this study's innovation.

Version 1:

Reviewer comments:

Reviewer #1

(Remarks to the Author)
The authors did a lot of work to the comment, which convinced me to change my mind. I can recommend its publication.

Reviewer #2

(Remarks to the Author)
The authors addressed my questions perfectly and I agree it to publish in Nature Communications.

Reviewer #3

(Remarks to the Author)
The authors have well addressed the concerns according to the reviewers' suggestions by providing supporting data and evidence with appropriate discussions, which further enhanced the quality of the manuscript. The reviewer thus suggests the acceptance of the revised manuscript.

Reviewer #4

(Remarks to the Author)
After the revision, the authors have made considerable efforts and devoted substantial length to address the issues we raised with scientific revisions and responses. Characterizations are also comprehensive to help understand this result. Therefore, this manuscript meets the high standards required for publication in the "Nature Communications" after addressing the following concerns.
Attention should be paid to the title. It is evident that this is a heterogeneous catalytic system; however, the title is highly misleading because it strongly suggests a homogeneous one. Therefore, TiOx or other substrates should be essential in this manuscript, including the title, all figures, and figure captions.

Reviewer #5

(Remarks to the Author)
The authors have positively responded all the comments raised by the reviewers. Therefore, I recommend the acceptance of this paper for publication.

Point-by-point responses to the reviewers' comments

The reviewers' comments are laid out below in *Italic font* and our responses are given in normal font and the changes/additions are highlighted in the revised manuscript with using blue colored text.

Reviewer #1 (Remarks to the Author):

This work presents an interesting study on heteronuclear dual-atom catalysts for NORR. However, I recommend rejection due to several significant concerns.

Response: Thank you for taking the time to review our manuscript and providing us with your insightful comments. We greatly appreciate your efforts in helping us enhance the quality of our research findings. All your comments were responded to in a thorough and transparent manner, which you will find below. We firmly believe that these revisions have substantially improved the quality of our manuscript. The corresponding revisions are described as follows:

1. First, the proposed mechanism relies heavily on computational models and indirect spectroscopic evidence. Direct experimental verification of the side-on Ti–N=O–Cu adsorption geometry under operating conditions is lacking. The in situ ATR-IRAS signals are insufficient to unambiguously assign this configuration.

Response: We thank the reviewer very much for these constructive comments. We agree that *in situ* ATR-IRAS alone may not provide definitive evidence to assign the side-on Ti–N=O–Cu adsorption configuration under operating conditions. To address this concern and provide stronger experimental support for the proposed Ti–N=O–Cu geometry (i.e., N adsorbed on Ti sites and O adsorbed on Cu sites), we have supplemented *in situ* Raman measurements in the revised manuscript. As shown in **Figure R1a-b**, besides the characteristic rutile TiO_2 peaks (E_g mode at 465 cm^{-1} and A_{1g} mode at 625 cm^{-1}) and the SO_4^{2-} signal at 979 cm^{-1}, a new peak at 218 cm^{-1} was clearly observed for both Ti–Ti and Cu_1–Ti pairs. This peak corresponds to the A_{1g} symmetry out-of-plane vibrations of Ti and N atoms, verifying the direct adsorption and coordination of N species on Ti sites (*J. Am. Chem. Soc.* **2025**, 147, 12, 10104–10117;

Nanoscale. **2016**, 8, 11385–11391; *Physical Review B.* **1978**, 17, 1095–1101.). The Cu–O Raman signal was not clearly detected in Cu_1–Ti pairs, probably due to the extremely low Cu loading and inherently weak scattering intensity of Cu–O species.

Besides, we also have supplemented ^{15}N-labeled NO *in situ* electrochemical attenuated total reflection infrared spectroscopy (ATR-IRAS) to more rigorously validate the assignment of *NO adsorption configuration. As displayed in **Figure R1c-d**, the peak near 1577 cm^{-1} for Cu_1–Ti shifts to a lower wavenumber of approximately 1548 cm^{-1} under a ^{15}NO atmosphere, whereas the peak for Ti–Ti shifts from 1737 cm^{-1} to 1712 cm^{-1}. Impressively, the peaks of *NO around 1548 cm^{-1} at Cu_1–Ti pairs and 1712 cm^{-1} at Ti−Ti pairs surface in ^{15}NO experiment matched well with the theoretical value (1577 cm^{-1} × 98.21% = 1549 cm^{-1} for Cu_1−Ti; 1737 cm^{-1} × 98.21% = 1706 cm^{-1} for Ti−Ti pairs). These isotopic shifts unambiguously assigned the peaks at 1577 cm^{-1} and 1737 cm^{-1} to a side-on and end-on NO adsorption mode, respectively.

Collectively, the complementary results from *in situ* Raman and isotope-labeled ATR-IRAS provide direct and consistent evidence for the proposed side-on Ti–N=O–Cu adsorption geometry under reaction conditions.

Figure R1a-b was added on **Page 32** in the revised Supporting Information as **Supplementary Figure S30**, **Figure R1c-d** was added on **Page 25** in the revised manuscript as **Figure 3c-d**, and the related discussion was added on **Page 9-11 Line 168-173** and **178-203** in the revised manuscript as follows:

"*In situ* Raman spectroscopy was then carried out to elucidate the surface response of active sites toward NO. A new peak at 218 cm^{-1}, corresponding to the A_{1g} symmetry out-of-plane vibrations of Ti and N atoms,[43, 44] was observed on both Ti−Ti and Cu_1−Ti pairs, thereby confirming the direct adsorption and coordination of N species on Ti sites. The Cu–O Raman signal was not clearly detected in Cu_1−Ti pairs, probably due to the extremely low Cu loading and inherently weak scattering intensity of Cu–O species."

"We further employed in situ differential electrochemical mass spectrometry (DEMS) to verify the NORR pathway over Ti−Ti and Cu_1−Ti pairs. As show in Figures 3b and S32,

gaseous species consistent with HNO/NOH (m/z = 31), NH_2OH (m/z = 33), NH_2 (m/z = 16), and NH_3 (m/z = 17) were detected for both samples, whereas no signal for atomic *N (m/z = 14) was observed, suggesting that Ti−Ti and Cu_1−Ti pairs followed a similar NORR reaction pathway.

In situ electrochemical attenuated total reflection infrared spectroscopy (ATR-IRAS) was performed identify adsorbed intermediates and clarify the reaction mechanism. Under applied potentials in a NO-saturated electrolyte, Ti−Ti pairs exhibited a weak adsorption peak at 1737 cm^{-1}, assigned to the end-on adsorbed NO.[46, 47] Moreover, the potential-dependent evolution of intermediates (Figure 3c-d) revealed characteristic bands for *NHO (1540, 1560 cm^{-1}),[2, 46] *NH_2OH (1181 cm^{-1}),[21, 47, 48, 49, 50] *NH_2 (1507 cm^{-1}),[21, 47, 51] and NH_3 (1457 cm^{-1}).[20, 21, 50] We proposed that NH_3 formation on both Ti−Ti and Cu_1−Ti pairs proceeds via the pathway: NO → *NHO → *NHOH → *NH_2OH → *NH_2 → NH_3.

The isotope labeling experiments using ^{15}NO was conducted to further confirm the NO adsorption configurations and reaction intermediates. Upon substituting the ^{14}NO with ^{15}NO, the peak at 1737 cm^{-1} appeared a pronounced redshift to 1712 cm^{-1}, close to the theoretically predicted N−O stretching frequency at 1706 cm^{-1}, based on the reduced mass in a simple harmonic oscillator model. Meanwhile, the *NHO peaks also exhibited two prominent isotopic redshifts of 16 cm^{-1} and 28 cm^{-1}, whereas shifts for other N-containing intermediates were indistinct, owing to the small frequency ratio ($\nu^{15}N/\nu^{14}N \approx 99.78\%$). Notably, Cu_1−Ti pairs displayed a side-on NO adsorption peak at 1577 cm^{-1}, which redshifted to 1548 cm^{-1} under the feedstock of ^{15}NO. The switching of NO adsorption from end-on to side-on configuration on Cu_1−Ti pairs, in agreement with our theoretical predictions, provided a dual-electron transfer channel via the proposed Ti–N=O–Cu adsorption motif for more effective *NO activation. Collectively, the complementary results from *in situ* Raman and isotope-labeled ATR-IRAS provide direct and consistent evidence for the proposed side-on Ti–N=O–Cu adsorption geometry under NORR reaction conditions (Figure 3e).”

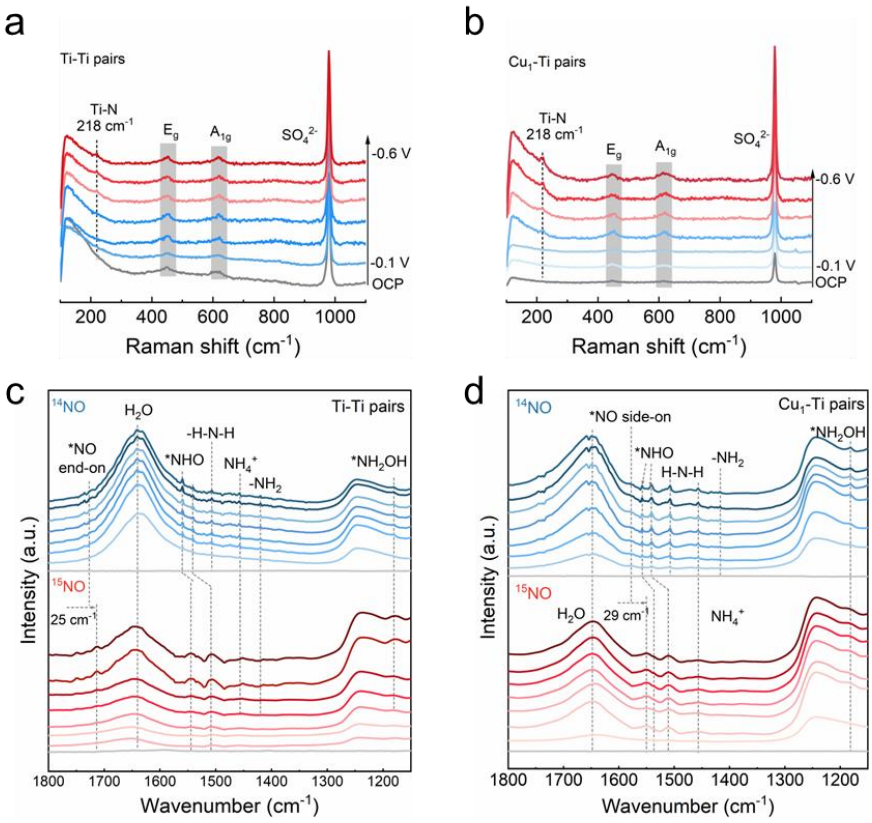

Figure R1. *In situ* electrochemical Raman spectra of (a) Ti–Ti pairs and (b) Cu_1−Ti pairs during NORR in 0.25 M K_2SO_4. *In situ* ATR-IRAS spectra of adsorbed NO species and intermediates using ^{14}NO and ^{15}NO isotopic labeling on (c) Ti–Ti pairs and (d) Cu_1−Ti pairs, collected at potentials stepped from open circuit potential to −0.6 V with an interval of −0.1 V in 0.25 M K_2SO_4.

2. Second, the catalyst synthesis is inadequately controlled. The formation of Cu–Ti pairs is inferred from EXAFS, but the possibility of small Cu clusters or oxides, especially after long-term testing, is not rigorously excluded. The post-stability characterization (XRD, XPS) is not convincing enough to confirm structural integrity.

Response: We thank the reviewer very much for these constructive comments. In this study, the formation of isolated Cu_1–Ti atomic pairs were comprehensively verified by using a combination of aberration-corrected HAADF-STEM and the Fourier-transform EXAFS. As shown in **Figure R2a**, the AC-HAADF-STEM images displayed uniformly bright contrast spots, confirming the highly dispersed characteristic of Cu atoms in the Cu_1–Ti pairs and ruling

out the generation of small Cu clusters or oxides. EXAFS results (**Figure R2c**) analysis further supported this conclusion. The main peak at ~1.50 Å corresponded to Cu–O bonds, while the distinct secondary peak at ~2.58 Å, situated between the reference positions for CuO and Cu_2O, was assigned to the Cu–Ti scattering path.

To address the concern regarding structural integrity after long-term testing, we performed post-stability characterization following 120 h of operation. As shown in **Figure R2b-c**, AC-HAADF-STEM images demonstrated no aggregation into clusters, and the Cu EXAFS spectrum retained the characteristic secondary peak at ~2.58 Å. These results strongly confirmed that the Cu–Ti pair structure remains intact and stable throughout the prolonged test.

Figure R2 was added on **Page 28** in the revised Supporting Information as **Supplementary Figure S26** and the related discussion was added on **Page 8 Line 146-147** in the revised manuscript as follows:

"This robust stability was also confirmed by post-reaction characterization with no notable changes in structure or composition (Figures S25-26)."

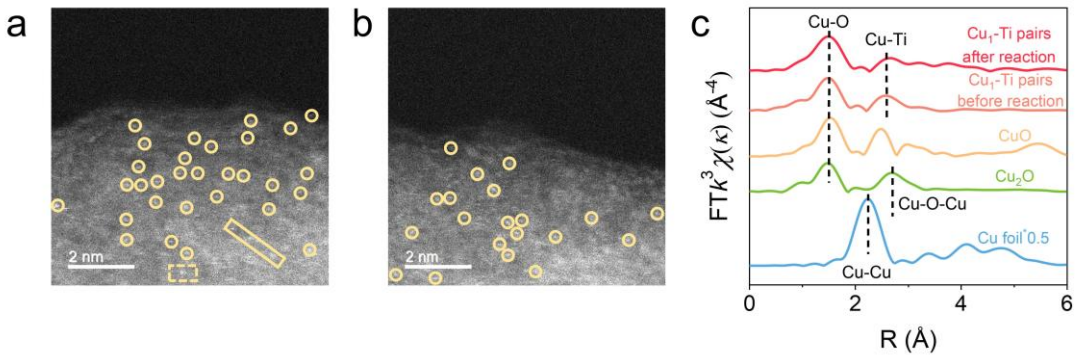

Figure R2. The HAADF-STEM images of the Cu_1–Ti pairs (a) before reaction and (b) after reaction. (c) FT-EXAFS spectra at the Cu K-edge for Cu_1–Ti pairs before and after the reaction.

3. Finally, the work does not sufficiently address selectivity. While NH_3 yield is high, potential by-products (e.g., N_2O, N_2, hydroxylamine) are not quantified or discussed. This omission weakens the practical relevance of the reported Faradaic efficiency.

Response: We thank the reviewer very much for these constructive comments regarding the product selectivity. During this revision, we first employed DEMS to detect the gaseous by-

products, including N_2 and N_2O. As shown in **Figure R3**, no characteristic signals corresponding to N_2 or N_2O were detected for either the Cu_1−Ti pairs or Ti−Ti pairs, suggesting that N_2 and N_2O were not generated during the NORR.

Subsequently, we used colorimetric assays to quantify the liquid-phase by-products including hydroxylamine (NH_2OH) and hydrazine (N_2H_4). The quantification of NH_2OH and N_2H_4 were performed according to Frear's method and the Watt-Chrisp method, respectively (*Nat. Synth.* **2025**, 4, 1598–1609; *Nat. Catal.* **2023**, 6, 949–958.). As shown in **Figure R4**, the highest concentration of NH_2OH was merely 0.01 μmol L^{-1} at −0.8 V vs. RHE, along with a Faradaic efficiency of 1.5%. Meanwhile, the concentration of formed N_2H_4 was below the detection limitation (5 μmol L^{-1}), suggesting the negligible generation of N_2H_4 during the NORR (**Figure R5**).

Figure R3, R4 and **R5** were added respectively on **Page 19-21** in the revised Supporting Information as **Supplementary Figure S17, S18** and **S19.** And the related discussion was added on **Page 7 Line 126-130** in the revised manuscript as follows:

"At this potential, the Cu_1−Ti pairs delivered an exceptional NH_3 yield of 189.9 μmol h^{-1} cm^{-2} with a FE_{NH3} of 93.7%, significantly outperforming the Ti−Ti pairs control (58.5 μmol h^{-1} cm^{-2}, 63.5% FE_{NH3}) and most reported NORR catalysts (Figure 2f, Table S2). Besides, NH_2OH was detected as the only byproduct with a corresponding Faradaic efficiency of 1.5% (Figures S17-19)."

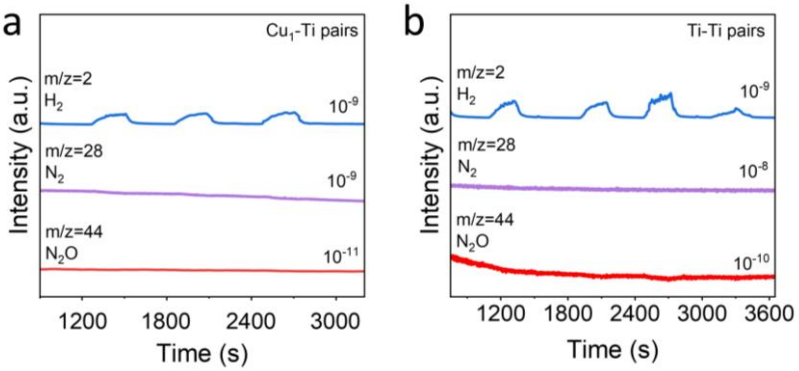

Figure R3. The signal spectrum of the intermediates on (a) Cu_1−Ti pairs and (b) Ti−Ti pairs monitored by DEMS during the NORR.

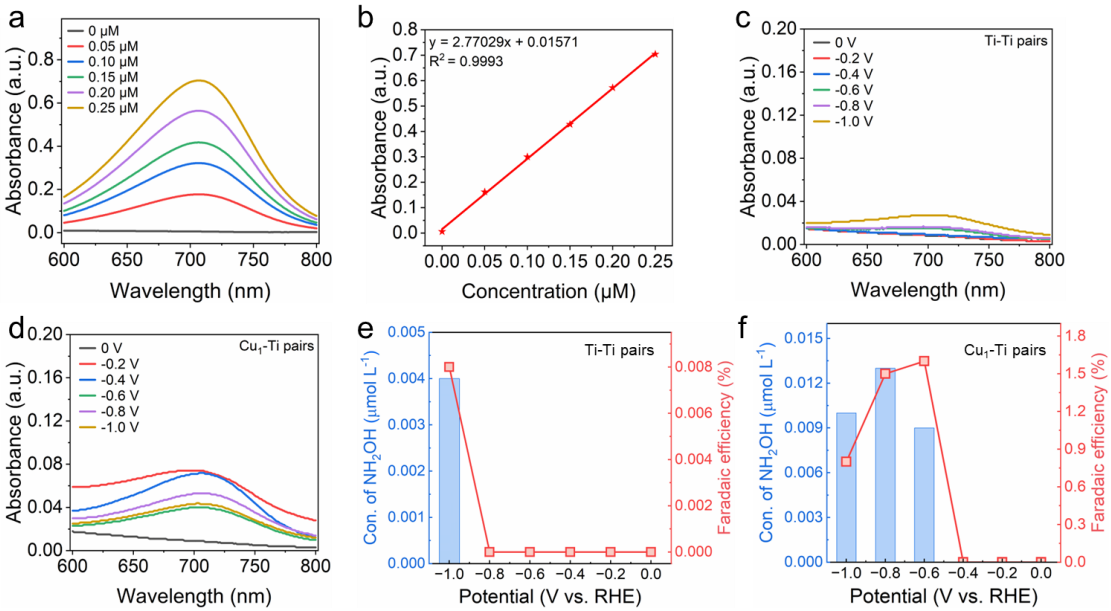

Figure R4. (a) UV-Vis absorption spectra of NH_2OH assays. (b) Calibration curve for quantitative calculation of NH_2OH concentrations. UV-Vis spectra for NH_2OH produced by (c) Ti−Ti pairs and (d) Cu_1−Ti. Corresponding NH_2OH concentration and Faradaic efficiency of (e) Ti−Ti and (f) Cu_1−Ti pairs.

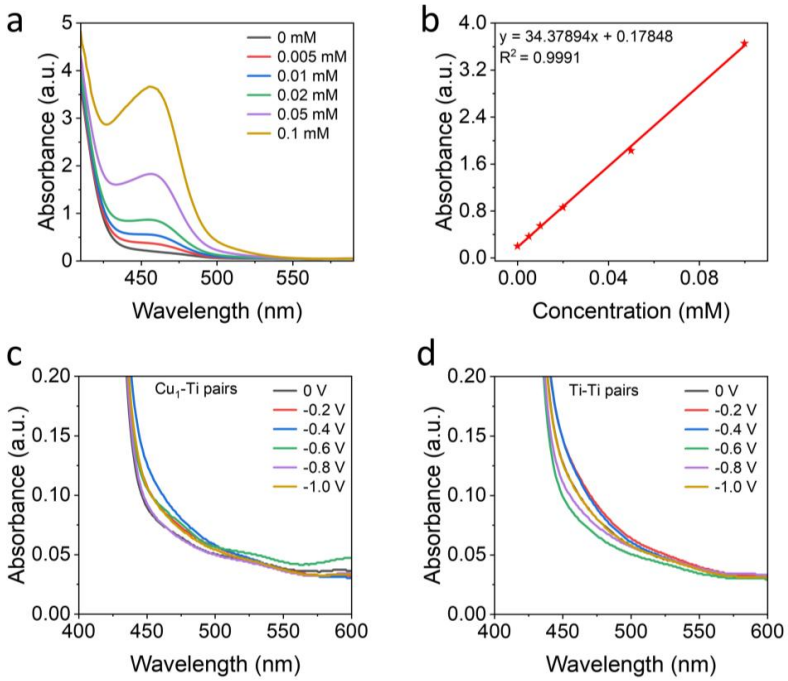

Figure R5. (a) UV-Vis absorption spectra of N_2H_4 assays. (b) Calibration curve for quantitative calculation of N_2H_4 concentrations. UV-Vis spectra for N_2H_4 produced by (c) Cu_1−Ti pairs and (d) Ti−Ti pairs.

Reviewer #2 (Remarks to the Author):

In this manuscript, the authors break away from the traditional single-site activation model of nitrogen oxide reduction reaction (NORR) and propose a design strategy for heteronuclear dual-sites cooperative catalysis. By leveraging the complementary affinities of Cu and Ti atoms toward O and N, they achieve a conformational shift of NO molecules from "end-on adsorption" to "side-on adsorption", which facilitates the efficient activation of polar NO molecules. This work emphasizes the significance of atomic-level design in creating asymmetric active sites capable of efficiently activating and converting polar molecules to high-value products. Overall, the paper is well-written, with a logical flow and clearly presented results. Therefore, I believe this manuscript is highly suitable for publication on Nature Communications after minor revisions.

Response: Thank you for taking the time to review our manuscript and providing us with your insightful comments. We greatly appreciate your efforts in helping us enhance the quality of our research findings. All your comments were responded to in a thorough and transparent manner, which you will find below. We firmly believe that these revisions have substantially improved the quality of our manuscript. The corresponding revisions are described as follows:

1. Given that NO can be oxidized to nitrate ions (NO_3^-) at the anode, which is then electro-reduced to ammonia at the cathode, a comparative analysis of the energy efficiency between the direct NO electro-reduction pathway and the indirect "NO→ NO_3^- → NH_3" pathway should be included.

Response: We greatly appreciate the reviewer's insightful and constructive comments about the energy efficiency of the direct NO electro-reduction pathway versus the "NO oxidation to nitrate → nitrate reduction" pathway.

First, we would like to clarify the key distinction between the two pathways lies in the number of electrons consumed during ammonia (NH_3) synthesis. Specifically, the direct NO electroreduction (NORR) pathway only requires 5 electrons per mole of NH_3 (NO + 4 H_2O +

5 e^- → NH_3 + 5 OH^-). In contrast, the "NO oxidation to nitrate → nitrate reduction" pathway involves two sequential steps: first, the oxidation of NO to nitrate (NO_3^-), followed by the electroreduction of NO_3^- to NH_3 (NO_3^- + 6 H_2O +8 e^- → NH_3 + 9 OH^-), which consumes a total of 8 electrons per mole of NH_3.

Since electron consumption is directly correlated with energy consumption in electrochemical reactions, the synthesis of one unit of NH_3 via the "NO oxidation to nitrate → nitrate reduction" pathway will inevitably consume more electrons, thereby resulting in higher energy consumption compared to the direct NORR pathway, even though the Faradaic efficiency of nitrate reduction exceeds 95%. This clearly indicates that the direct NO electroreduction pathway is more energy-efficient than the indirect pathway involving nitrate as an intermediate.

2. Since NORR typically yields multiple products (e.g., hydrazine and hydroxylamine), the authors should specify whether other byproducts were detected during testing. If so, corresponding characterization data and quantitative results must be provided.

Response: We thank the reviewer for this constructive suggestion. We used colorimetric assays to quantify the liquid-phase byproducts hydroxylamine (NH_2OH) and hydrazine (N_2H_4).

Detection of NH_2OH: The concentration of NH_2OH was determined according to Frear's method (*Nat. Synth.* **2025**, 4, 1598–1609). The standard solution was prepared by diluting the mother liquor (0.5 mM NH_2OH·HCl aqueous solution containing 0.25 M K_2SO_4). First, 1 mL of standard solution was placed in a clean centrifuge tube. Then, 1 mL of 0.1 M PBS solution, 1 mL deionized water and 0.2 mL of 12 wt% trifluoroacetic acid were added in order, followed by 1 mL of 10 g L^{-1} 8-quinolinol ethanol solution. Finally, 1 mL of 1 M Na_2CO_3 solution was added. The vials were then placed in a 60 °C oven for 15 min and cooled for another 10 min. The absorption spectrum was recorded on an UV–vis spectrophotometer in the wavelength range 600–800 nm. The solution without NH_2OH·HCl was used for background correction. The absorbances were recorded at a wavelength of 705 nm and plotted against the hydroxylamine concentrations. The test of the target sample follows the same process as the

standard solution.

As shown in **Figure R6**, the highest concentration of NH_2OH was determined to be 0.01 μmol L^{-1} with a faradaic efficiency of 1.5% at the potential of −0.8 V vs. RHE.

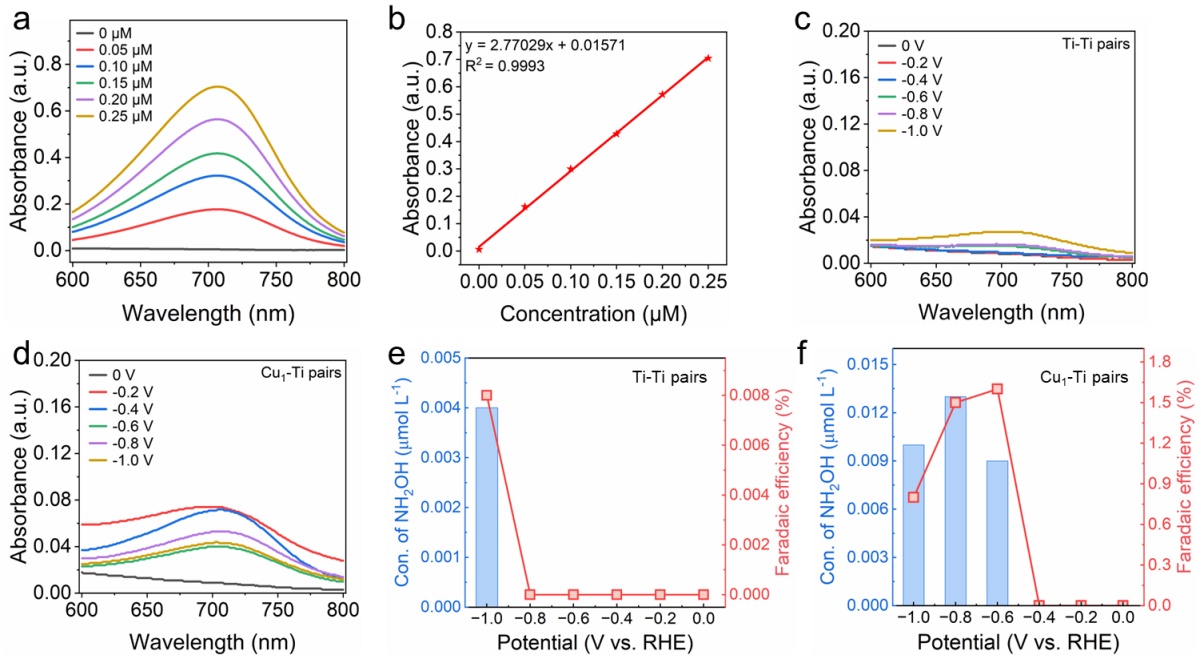

Figure R6. (a) UV-Vis absorption spectra of NH_2OH assays. (b) Calibration curve for quantitative calculation of NH_2OH concentrations. UV-Vis spectra for NH_2OH produced by (c) Ti−Ti pairs and (d) Cu_1−Ti. Corresponding NH_2OH concentration and Faradaic efficiency of (e) Ti−Ti and (f) Cu_1−Ti pairs.

Detection of N_2H_4: The possible N_2H_4 product in the electrolyte solution was measured by the Watt-Chrisp method. Briefly, 10 mL of HCL, 2 g of para-(dimethylamino) benzaldehyde and 100 mL of C_2H_5OH were dissolved and used as a sensitive chromogenic reagent. Then, 2 mL of solution product was collected from the cathode compartment and uniform mixed with 5 mL of the chromogenic reagent at room temperature. After standing for 20 min in the dark for at room temperature, the light absorbance of the resulting solution was detected by UV-Vis spectrophotometer at the wavelength of 457 nm.

As shown in **Figure R7**, the concentration of formed N_2H_4 was below the detection limitation (5 μmol L^{-1}), suggesting the negligible generation of N_2H_4 during the NORR.

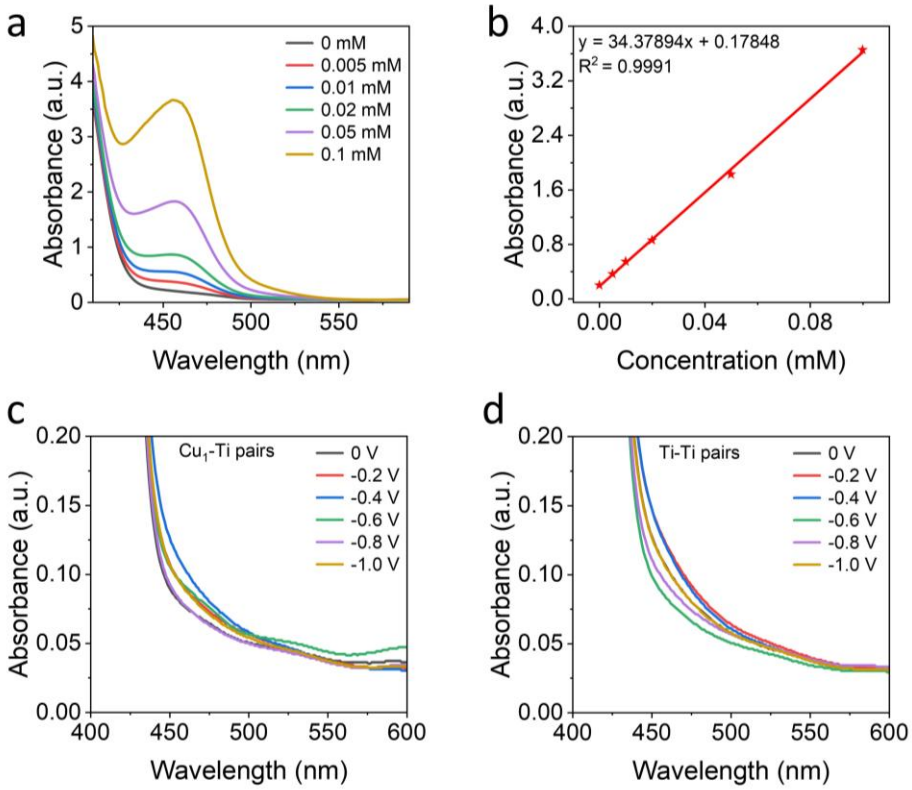

Figure R7. (a) UV-Vis absorption spectra of N_2H_4 assays. (b) Calibration curve for quantitative calculation of N_2H_4 concentrations. UV-Vis spectra for N_2H_4 produced by (c) Cu_1−Ti pairs and (d) Ti−Ti pairs.

During this revision, **Figure R6** and **R7** were added on **Page 19-21** in the revised Supporting Information as **Supplementary Figure S17, S18** and **S19**, respectively**.** And the related discussion was added on **Page 7 Line 126-130** in the revised manuscript as follows:

"At this potential, the Cu_1−Ti pairs delivered an exceptional NH_3 yield of 189.9 μmol h^{-1} cm^{-2} with a FE_{NH3} of 93.7%, significantly outperforming the Ti−Ti pairs control (58.5 μmol h^{-1} cm^{-2}, 63.5% FE_{NH3}) and most reported NORR catalysts (Figure 2f, Table S2). Besides, NH_2OH was detected as the only byproduct with a corresponding Faradaic efficiency of 1.5% (Figures S17-19)."

Besides, the detect methods for NH_2OH and N_2H_4 were respectively added on **Pages 44-45** in the revised Supporting Information as **Supplementary Note 6** and **Supplementary Note 7** as follows:

"The concentration of NH_2OH was determined according to Frear's method. The standard solution was prepared by diluting the mother liquor (0.5 mM $NH_2OH{\cdot}HCl$ aqueous solution containing 0.25 M K_2SO_4). First, 1 mL of standard solution was placed in a clean centrifuge tube. Then, 1 mL of 0.1 M PBS solution, 1 mL deionized water and 0.2 mL of 12 wt% trifluoroacetic acid were added in order, followed by 1 mL of 10 g L^{-1} 8-quinolinol ethanol solution. Finally, 1 mL of 1 M Na_2CO_3 solution was added. The vials were then placed in a 60 °C oven for 15 min and cooled for another 10 min. The absorption spectrum was recorded on an UV–vis spectrophotometer in the wavelength range 600–800 nm. The solution without $NH_2OH{\cdot}HCl$ was used for background correction. The absorbances were recorded at a wavelength of 705 nm and plotted against the hydroxylamine concentrations. The test of the target sample follows the same process as the standard solution.

The possible N_2H_4 product in the electrolyte solution was measured by the Watt-Chrisp method. Briefly, 10 mL of HCL, 2 g of para-(dimethylamino) benzaldehyde and 100 mL of C_2H_5OH were dissolved and used as a sensitive chromogenic reagent. Then, 2 mL of solution product was collected from the cathode compartment and uniform mixed with 5 mL of the chromogenic reagent at room temperature. After standing for 20 min in the dark for at room temperature, the light absorbance of the resulting solution was detected by UV-Vis spectrophotometer at the wavelength of 457 nm."

3. The supplementary information should detail the calculation methodology for the "ECSA-normalized activity," along with a corresponding figure, to enable direct comparison with prior studies.

Response: We thank the reviewer for this constructive comment. During this revision, we provided detailed calculation steps regarding the "ECSA-normalized activity" as follows:

Determination of Double-Layer Capacitance (C_{dl}): As described in the main text (Electrochemical measurement), cyclic voltammetry (CV) scans were performed in a non-Faradaic potential region at various scan rates (20, 40, 60, 80, 100 mV s^{-1}). Subsequently, plot a scatter diagram with the scanning speed as the horizontal axis and the current density

difference (Δj) at the voltage center as the vertical axis. The slope of the linear fit represents 2*C_{dl}. As shown in **Figure R8**, the specific capacitance of the Cu_1−Ti pairs and Ti−Ti pairs were 0.886 mF cm^{-2} and 0.443 mF cm^{-2}, respectively.

Calculation of Electrochemical Active Surface Area (ECSA): The ECSA was calculated using the formula: ECSA = C_{dl}/C_s, where Cs denotes the specific capacitance. For a flat surface, Cs is generally found to be in the range of 20~60 μF cm^{-2}. In the following calculations of the electrochemically active surface area, we assumed that the Cs was 40 μF cm^{-2}, and the ECSAs of the two samples were calculated as follows:

$$A_{ECSA}^{Cu_1\text{-Ti pairs}} = \frac{0.886\ \text{mF cm}^{-2}}{40\ \mu\text{F cm}^{-2}\ \text{per cm}^2_{ECSA}} = 22.15\ \text{cm}^2_{ECSA}$$

$$A_{ECSA}^{\text{Ti-Ti pairs}} = \frac{0.443\ \text{mF cm}^{-2}}{40\ \mu\text{F cm}^{-2}\ \text{per cm}^2_{ECSA}} = 11.08\ \text{cm}^2_{ECSA}$$

The ECSA-normalized activity was calculated as follows:

$$\text{ECSA-normalized activity } (Cu_1\text{-Ti pairs}) = \frac{189.9\ \mu\text{mmol h}^{-1}\ \text{cm}^{-2}*4\ \text{cm}^2}{22.15\ \text{cm}^2_{ECSA}}$$

$$= 34.29\ \mu\text{mmol h}^{-1}\ \text{cm}^{-2}_{ECSA}$$

$$\text{ECSA-normalized activity (Ti-Ti pairs)} = \frac{58.5\ \mu\text{mmol h}^{-1}\ \text{cm}^{-2}*4\ \text{cm}^2}{11.08\ \text{cm}^2_{ECSA}}$$

$$= 21.13\ \mu\text{mmol h}^{-1}\ \text{cm}^{-2}_{ECSA}$$

Therefore, the resulting ECSA-normalized activity of the Cu_1−Ti pairs was 1.6 times greater than that of the Ti−Ti pairs (**Figure R9**).

Figure R9 was added on **Page 24** in the revised Supporting Information as **Supplementary Figure S22.**

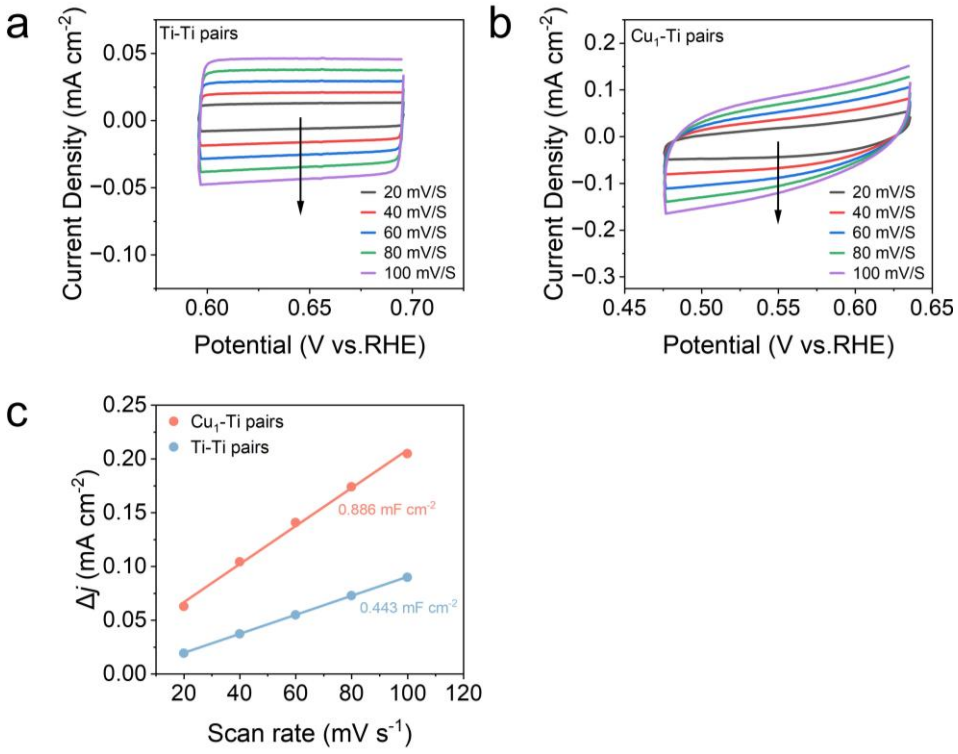

Figure R8. CV curves of (a) Ti−Ti pairs and (b) Cu_1−Ti pairs under different scan rates from 20 to 100 mV s^{-1}. (c) Plots of the current density difference (Δj) at the centered potential plotted against the scan rate. The slope of the fitted straight line is twice value of the electrical double-layer capacitor value.

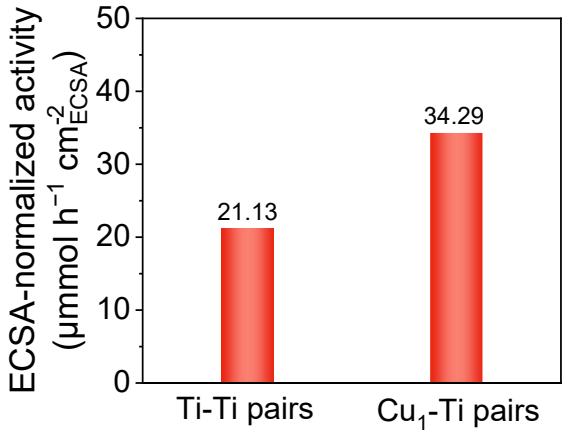

Figure R9. The ECSA-normalized NH_3 yield of Ti−Ti pairs and Cu_1−Ti pairs.

4. Aberration-corrected SEM analysis of post-reaction catalyst structure is necessary to verify the retention of the Cu single-atom configuration.

Response: Thank you for your valuable suggestions. As shown in **Figure R10**, aberration-corrected high-angle annular dark-field scanning transmission electron microscopy (AC HAADF-STEM) image clearly showed that the distinct small bright spots are observable in used Cu_1−Ti pairs, indicating that the Cu single-atom dispersion is well maintained without aggregation or migration during the NORR reaction.

Figure R10 was added on **Page 28** in the revised Supporting Information as **Supplementary Figure S26b** and the related discussion was added on **Page 8 Line 146-147** in the revised manuscript as follows:

"This robust stability was also confirmed by post-reaction characterization with no notable changes in structure or composition (Figures S25-26)."

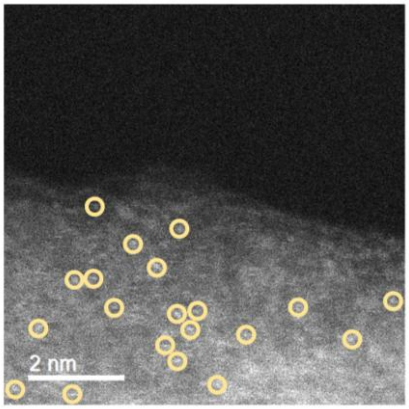

Figure R10. The HAADF-STEM images of the Cu_1−Ti pairs after testing.

5. Thermodynamic data (ΔE, ΔEZPE, and ΔS) should be included within the supplementary information to facilitate reproduction of theoretical results. In addition, in the supplementary XPS spectra, orbital symbols (e.g., 2p, 3d) should be presented in italics. To ensure accuracy, the authors should also meticulously review all figure and table information.

Response: We thank the reviewer for the comment and suggestion. Following the reviewer's advice, we have compiled the thermodynamic data (ΔE, ZPE, TS and ΔG) for each intermediate of the NORR pathway on the Ti–Ti pairs and Cu_1–Ti pairs catalyst. We now provide the following data in **Table R1**.

During this revision, **Table R1** was added on **Page 50** in the revised Supporting Information as **Supplementary Table S3.**

		ΔE (eV)	ZPE (eV)	TS (eV)	ΔG (eV)
Gas	NO(g)	/	0.11	0.64	/
	H_2O(g)	/	0.58	0.59	/
	H_2(g)	/	0.33	0.40	/
Ti–Ti pairs	*NO	-1.67	0.22	0.11	-1.06
	*NHO	-1.20	0.47	0.18	-0.40
	*HNOH	-2.12	0.78	0.12	-0.98
	*NH_2OH	-3.98	1.08	0.12	-2.54
	*NH_2	-3.54	0.65	0.11	-2.44
Cu_1–Ti pairs	*NO	-1.90	0.17	0.14	-1.36
	*NHO	-2.90	0.48	0.13	-2.05
	*HNOH	-3.30	0.79	0.15	-2.16
	*NH_2OH	-3.34	1.13	0.21	-1.90
	*NH_2	-5.35	0.70	0.08	-4.18

Table R1. Calculated ΔE, ZPE, TS and ΔG for each intermediate of the NORR pathway on the Ti–Ti pairs and Cu_1–Ti pairs catalyst.

Besides, we have revised the supplementary XPS spectra to ensure that all orbital symbols (e.g., *2p, 3d*) are presented in italics to adhere to the standard scientific notation. The changes have been made in the revised Supplementary Information file. Upon thorough review, we identified and corrected the following discrepancies:

1. The labels for the horizontal coordinate X in **Figure 1h** and **Figure 1i** have been corrected from "R+α (Å)" to "R (Å)".

2. The captions for **Figures 3a–3d** contain errors. The images have been reorganized and reordered for clarity.

3. In **Table S1** of the supplementary information, "Cu-Cu" has been corrected to "Cu-Ti (Cu-O-Ti)".

Reviewer #3 (Remarks to the Author):

In this manuscript, Zhang et al. report the fabrication of Cu_1-Ti catalytic pairs on commercial titanium felt. This design is specifically tailored for the electrocatalytic reduction of NO to NH_3. They discovered that unlike the end-on adsorption mechanism of NO on symmetric Ti-Ti pairs, the asymmetric Cu_1-Ti pairs enable a novel side-on bidentate adsorption pathway. This adsorption behavior activates both ends of the N=O bond simultaneously, thereby promoting efficient activation of NO molecules and ultimately achieving high selectivity and yield in ammonia production.

The authors have systematically integrated experimental characterization, in situ spectroscopic analysis, and DFT calculations to elucidate the heteronuclear bidentate synergistic catalytic mechanism underlying the observed performance. On this basis, I recommend the publication of this manuscript in Nature Communications following appropriate revisions. Specific comments for revision are provided below..

Response: Thank you for taking the time to review our manuscript and providing us with your insightful comments. We greatly appreciate your efforts in helping us enhance the quality of our research findings. All your comments were responded to in a thorough and transparent manner, which you will find below. We firmly believe that these revisions have substantially improved the quality of our manuscript. The corresponding revisions are described as follows:

1. Why was Cu chosen to form the Cu_1-Ti pairs catalytic system? Are Fe_1-Ti pairs, Co_1-Ti pairs, or Ni_1-Ti pairs feasible? Please provide corresponding explanations.

Response: We thank the reviewer for this insightful question regarding the choice of Cu for constructing the Cu_1−Ti pairs and the feasibility of other transition metals (Fe, Co, Ni). We chose Cu to construct the Cu_1−Ti atomic pair catalytic system based on comprehensive considerations of unique electronic properties and experimental validation, with detailed explanations as follows:

The unique electronic properties of Cu: Compared with Fe, Co, and Ni, Cu possesses a

fully filled and stable $3d^{10}$ electronic configuration. Its 3d orbitals show excellent energy matching with the $2\pi^*$ orbitals of NO, enabling the formation of a moderate back-donating π bond. This interaction effectively activates the N=O bond while avoiding excessive adsorption and subsequent product poisoning. Moreover, the high hydrogen evolution reaction (HER) overpotential of Cu guarantees superior selectivity toward the nitric oxide reduction reaction (NORR). (*Angew. Chem. Int. Ed.* **2020**, 59, 9711−9718; *J. Am. Chem. Soc.* **2022**, 144, 1258−1266).

Experimental validation: Our control experiments comparing Cu_1−Ti pairs with Fe_1−Ti pairs, Co_1−Ti pairs, and Ni_1−Ti pairs (synthesized using the same method) showed that Cu_1−Ti indeed exhibited the highest NORR activity and faradaic efficiency (as shown in **Figure R11**).

Figure R11 was added on **Page 29** in the revised Supporting Information as **Supplementary Figure S27** and the related discussion was added on **Page 8 Line 147-153** in the revised manuscript as follows:

"To evaluate the appliable potential of heterogeneous catalytic pairs for the NORR, we synthesized other M_1−Ti pairs (where M was Fe, Co and Ni). All these M_1−Ti pairs exhibited enhanced NORR performance compared with the Ti−Ti pairs, among which the Cu_1−Ti pairs demonstrated the best performance (Figure S27). These results confirmed that the proposed heteronuclear dual-atom sites NO activation strategy was effective, and Cu_1−Ti pairs are particularly superior, as the unique 3d orbitals of Cu could effectively weaken the N=O bond via the favorably bidirectional "donation-backdonation" mechanism."

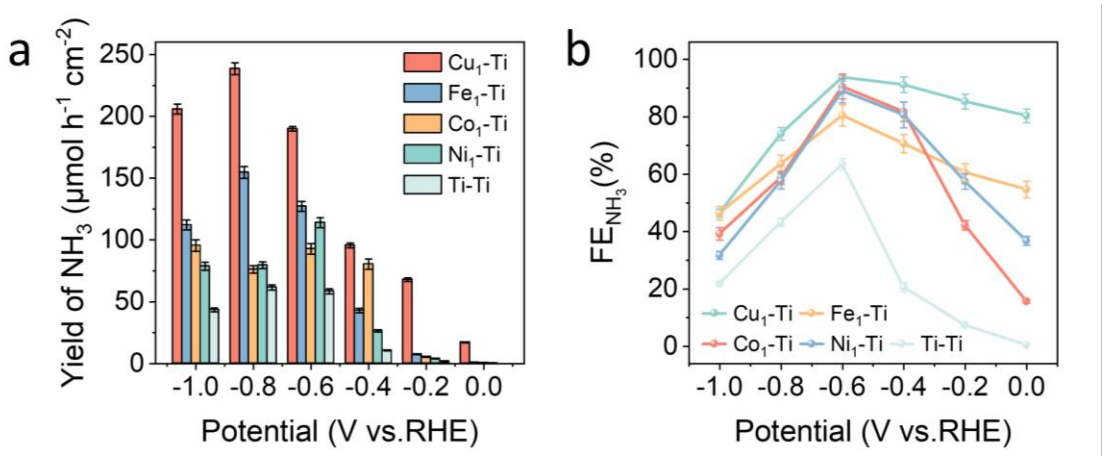

Figure R11. (a) NH_3 yield rate of Cu_1−Ti, Fe_1−Ti, Co_1−Ti, Ni_1−Ti and Ti−Ti at different potentials. (b) NH_3 FEs of Cu_1−Ti, Fe_1−Ti, Co_1−Ti, and Ni_1−Ti and Ti−Ti at different potentials.

2. The specific contribution of the Cu-O-Ti shell in the FT-EXAFS R space needs to be determined to more clearly elucidate the Cu-O-Ti coordination relationship.

Response: We thank the reviewer for this valuable suggestion to clarify the contribution of the Cu−O−Ti shell in the R space of FT-EXAFS. Following this advice, we have re-analyzed our EXAFS data. **Figure 1h and Figure 1i** show the Fourier-transformed (FT) k^3-weighted Cu K-edge EXAFS spectrum of our Cu_1−Ti pairs, along with the best fit in R space. Below we provide a detailed determination of this coordination relationship:

Data preprocessing: The raw EXAFS data was processed via Athena software, including background subtraction, normalization, and k^3-weighting to enhance the signal of high-coordination shells.

Fourier transform (FT) to R space: The k^3-weighted $\chi(k)$ was Fourier-transformed into R space in the range of k = 2.0-12.0 Å^{-1}, yielding the radial distribution function (RDF) of the local structure around Cu atoms.

Multi-shell fitting in R space: We performed multi-shell fitting of the FT-EXAFS spectrum in R space using Artemis software, with theoretical scattering paths calculated by FEFF. We separated the contributions of different shells. As presented in **Table R2**, the peak at R = 1.50 Å (uncorrected for phase shift, corresponding to actual bond length ~1.96 Å) was assigned to the Cu-O first coordination shell. The peak at R = 2.58 Å (uncorrected for phase shift, actual bond length ~3.0 Å) was confirmed as the Cu−Ti (Cu−O−Ti) shell; this peak originates from the scattering path where photoelectrons are scattered by neighboring Ti atoms, which is the key signal reflecting the Cu−Ti (Cu−O−Ti) coordination relationship (*Nano Energy.* **2022**, 103, 107853; *Nat Commun*. **2023**, 14, 1117; *Nat Commun*. **2025**, 16, 665).

Samples	Path	N	R (Å)	σ2 (Å^{-2})	ΔE_0 (eV)	R-factor
Cu foil	Cu-Cu	12	2.54 ± 0.01	0.0087	4.3 ± 0.5	0.0033
Cu_1-Ti pairs	Cu-O	3.90 ± 0.20	1.96 ± 0.01	0.0062	−3.6 ± 1.1	0.0114
	Cu-Ti (Cu-O-Ti)	5.00 ± 0.60	3.02 ± 0.01	0.0150		

Table R2. The fitted EXAFS data for Cu foil and Cu_1−Ti pairs samples.

3. *What is the Cu-Ti distance in Cu_1-Ti pairs? From a theoretical perspective, how does this distance influence the adsorption configuration?*

Response: We thank the reviewer for this important comment. By compressing or stretching the lattice, we controlled the Cu−Ti distance in Cu_1−Ti pairs and calculated the corresponding adsorption energies of NO in side-on and end-on configurations, respectively (**Figure R12**).

When the Cu–Ti pair distance was short, the adsorption energy of NO in the end-on configuration was −1.28 eV, while the side-on configuration could not be located during energy minimization, indicating that the most stable adsorption configuration of NO under this condition was end-on. When the Cu–Ti pair distance was long, the adsorption energy of NO in the end-on configuration was −5.07 eV, which was more exothermic than that of the side-on configuration (−3.37 eV), again suggesting that the end-on configuration was the most stable. Only when the Cu–Ti distance was moderate does the side-on configuration became thermodynamically more favorable, with an adsorption energy of −1.97 eV, which was less negative than that of the end-on configuration (−0.81 eV). These results mainly originated from the different degrees of orbital matching between the Cu–Ti distance and the NO molecule at different distances. Only at a moderate Cu–Ti distance, the d_{xy}/d_{yz} orbitals of Cu and Ti

exhibited the highest degree of matching with the π orbitals of the NO molecule, hybridizing into more stable orbitals.

Consequently, the side-on adsorption configuration of NO became thermodynamically favored over the end-on configuration and emerges as the most stable adsorption mode. This also leaded to the polar NO molecule adsorbed in the side-on configuration on the Cu–Ti distance being activated rather than stabilized, as compared to the end-on configuration, which switched the free energy of *NO hydrogenation to *NHO from an uphill Gibbs free energy change to a downhill free energy change, ultimately enabling an exceptional NH_3 yield as we reported.

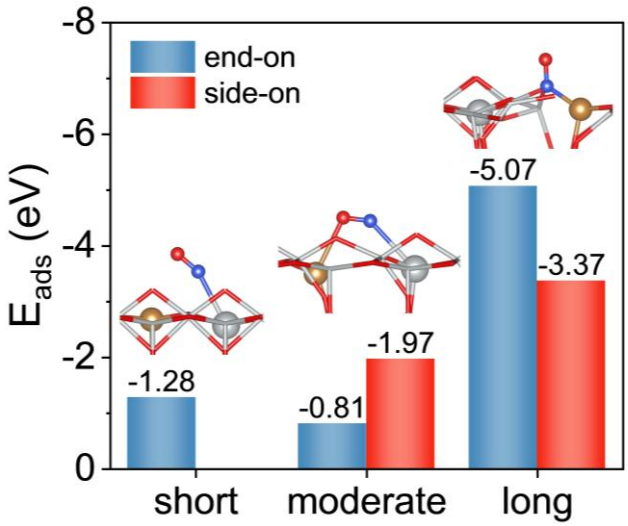

Figure R12. Adsorption energies of NO in end-on and side-on configurations on Cu_1−Ti pairs with different spacings.

4. In poisoning experiments, the SCN^- poisoning test involves adding SCN^- directly to the electrolyte, while the S^{2-} poisoning test employs an electrode immersion and rinsing procedure. What are the considerations behind these different approaches?

Response: We thank the reviewer for raising this insightful question regarding the different procedures used in our poisoning experiments (SCN^- vs. S^{2-}). The distinct approaches are indeed by design, based on the fundamental differences in the chemical nature of these two poisoning agents and their interaction with the catalytic sites.

For the SCN^- poisoning test, SCN^- was directly added into the electrolyte during the NORR tests (*J. Phys. Chem. Lett.* **2011**, 2, 295–298). SCN^- is chemically stable and exhibits strong, non-selective adsorption toward almost all active sites, including single-atom Cu sites and Ti sites on the TiO_x support. Direct addition enables real-time inhibition of active sites during electrocatalysis, allowing us to identify the overall contribution of active sites under operating conditions. (*ACS Catal.* **2025**, 15, 11705–11715).

For the S^{2-} poisoning test, we adopted a pre-immersion and rinsing strategy rather that direct addition. This design arises from the extremely high and specific affinity of S^{2-} toward Cu sites over other metal sites (*J. Phys. Chem. C.* **2014**, 118, 24583–24590). By immersing the catalyst in a S^{2-} solution, we can ensure that S^{2-} has sufficient time to specifically adsorb to the Cu metal sites. The subsequent rinsing step removes weakly adsorbed species, eliminating interference from free S^{2-} in the NORR electrolyte. In this way, the observed activity attenuation can be unambiguously attributed to the strong and specific binding between S^{2-} and Cu active sites.

5. Hydroxylamine can serve both as an intermediate and as the final product of NORR. Distinct hydroxylamine signals appear in the infrared spectrum. Please indicate whether the product contains hydroxylamine or other non-ammonia substances.

Response: We thank the reviewer very much for these constructive comments regarding the product selectivity. We used colorimetric assays to quantify the hydroxylamine (NH_2OH) duing the NORR. The quantification of NH_2OH was performed according to Frear's method (*Nat. Synth.* **2025**, 4, 1598–1609). As shown in **Figure R13**, the highest concentration of NH_2OH was merely 0.01 μmol L^{-1} at −0.8 V vs. RHE, along with a Faradaic efficiency of 1.5%.

Other non-ammonia substances including N_2, N_2O and hydrazine (N_2H_4) were identified in this revision. DEMS was conducted to detect the gaseous by-products, including N_2 and N_2O. As shown in **Figure R14**, no characteristic signals corresponding to N_2 or N_2O were observed for either the Cu_1−Ti pairs or Ti−Ti pairs, suggesting that N_2 and N_2O were not generated during the NORR.

Subsequently, N_2H_4 was quantified by means of colorimetric assays, according to the Watt-Chrisp method (*Nat. Synth.* **2025**, 4, 1598–1609; *Nat. Catal.* **2023**, 6, 949-958.). As shown in **Figure R15**, the concentration of formed N_2H_4 was below the detection limitation (5 μmol L^{-1}), suggesting the negligible generation of N_2H_4 during the NORR.

Figure R13, R14 and **R15** were added on **Page 19-21** in the revised Supporting Information as **Supplementary Figure S17, S18** and **S19**, respectively**.** And the related discussion was added on **Page 7 Line 126-130** in the revised manuscript as follows:

"At this potential, the Cu_1−Ti pairs delivered an exceptional NH_3 yield of 189.9 μmol h^{-1} cm^{-2} with a FE_{NH3} of 93.7%, significantly outperforming the Ti−Ti pairs control (58.5 μmol h^{-1} cm^{-2}, 63.5% FE_{NH3}) and most reported NORR catalysts (Figure 2f, Table S2). Besides, NH_2OH was detected as the only byproduct with a corresponding Faradaic efficiency of 1.5% (Figures S17-19)."

Besides, the detect methods for NH_2OH and N_2H_4 was added on **Page 44-45** in the revised Supporting Information as **Supplementary Notes 6-7** as follows:

"The concentration of NH_2OH was determined according to Frear's method. The standard solution was prepared by diluting the mother liquor (0.5 mM $NH_2OH{\cdot}HCl$ aqueous solution containing 0.25 M K_2SO_4). First, 1 mL of standard solution was placed in a clean centrifuge tube. Then, 1 mL of 0.1 M PBS solution, 1 mL deionized water and 0.2 mL of 12 wt% trifluoroacetic acid were added in order, followed by 1 mL of 10 g L^{-1} 8-quinolinol ethanol solution. Finally, 1 mL of 1 M Na_2CO_3 solution was added. The vials were then placed in a 60 °C oven for 15 min and cooled for another 10 min. The absorption spectrum was recorded on an UV–vis spectrophotometer in the wavelength range 600–800 nm. The solution without $NH_2OH{\cdot}HCl$ was used for background correction. The absorbances were recorded at a wavelength of 705 nm and plotted against the hydroxylamine concentrations. The test of the target sample follows the same process as the standard solution."

"The N_2H_4 product in the electrolyte solution was measured by the Watt-Chrisp method. Briefly, 10 mL of HCL, 2 g of para-(dimethylamino) benzaldehyde and 100 mL of C_2H_5OH were dissolved and used as a sensitive chromogenic reagent. Then, 2 mL of solution product

was collected from the cathode compartment and uniform mixed with 5 mL of the chromogenic reagent at room temperature. After standing for 20 min in the dark for at room temperature, the light absorbance of the resulting solution was detected by UV-Vis spectrophotometer at the wavelength of 457 nm."

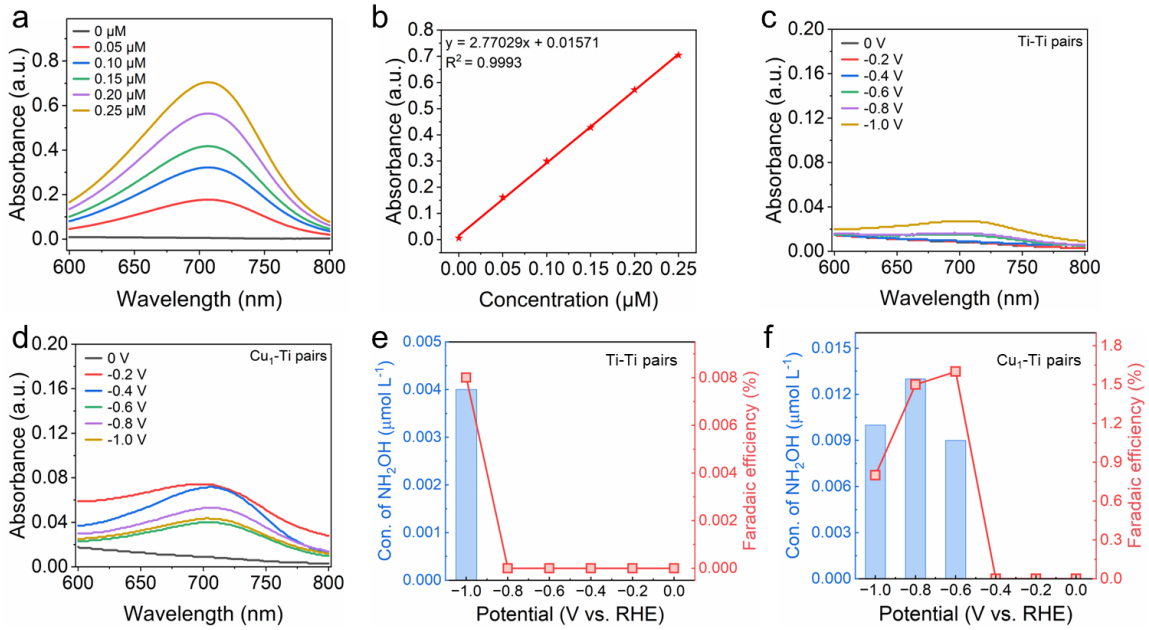

Figure R13. (a) UV-Vis absorption spectra of NH_2OH assays. (b) Calibration curve for quantitative calculation of NH_2OH concentrations. UV-Vis spectra for NH_2OH produced by (c) Ti−Ti pairs and (d) Cu_1−Ti. Corresponding NH_2OH concentration and Faradaic efficiency of (e) Ti−Ti and (f) Cu_1−Ti pairs.

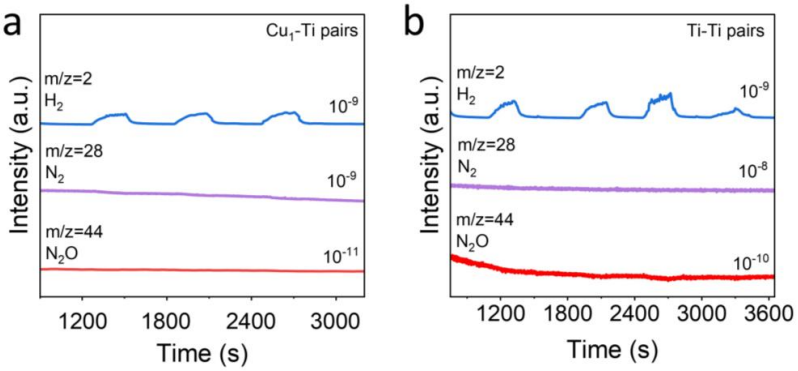

Figure R14. The signal spectrum of the intermediates on (a) Cu_1−Ti pairs and (b) Ti−Ti pairs monitored by DEMS during the NORR.

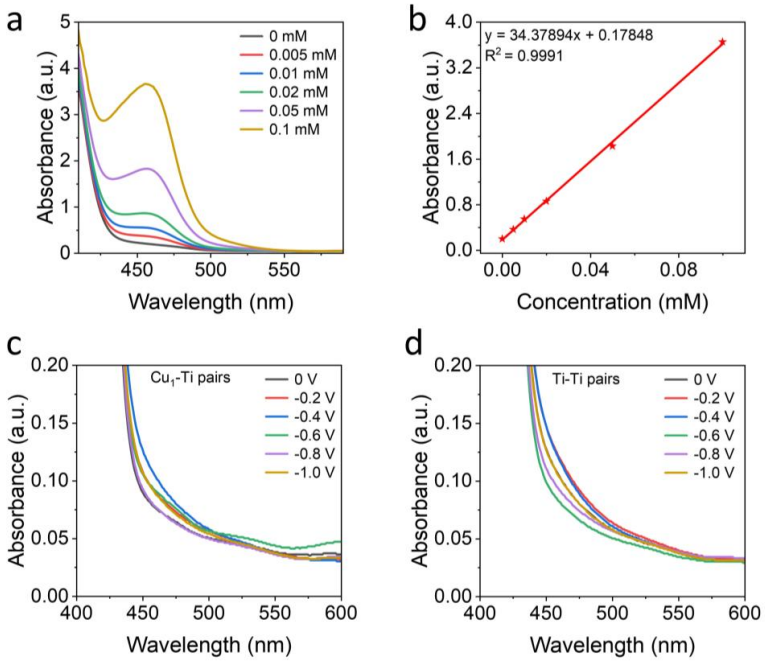

Figure R15. (a) UV-Vis absorption spectra of N_2H_4 assays. (b) Calibration curve for quantitative calculation of N_2H_4 concentrations. UV-Vis spectra for N_2H_4 produced by (c) Cu_1−Ti pairs and (d) Ti−Ti pairs.

6. Certain figures appear to be mislabeled or incorrectly captioned. The authors should verify that all figure labels and legends accurately correspond to the data presented.

Response: We sincerely appreciate this careful and valuable comment. We have thoroughly verified all figures, captions and legends in the revised manuscript, corrected all mislabeled elements and inaccurate captions, and ensured that all figure labels, legends and captions are fully consistent with the presented data. The detailed revisions are summarized as follows:

(a) The orbital symbols (e.g., *p*, *d*) of supplementary XPS spectra have been revised italics to ensure the standard scientific notation.

(b) The labels for the horizontal coordinate X in Figure 1h and Figure 1i have been corrected from "R+α (Å)" to "R (Å)".

(c) The Figures 3a–3d have been reorganized and reordered for clarity.

(d) In Table S1 of the supplementary information, "Cu-Cu" has been corrected to "Cu-Ti (Cu-O-Ti)".

Reviewer #4 (Remarks to the Author):

In this manuscript, the authors ingeniously designed a bimetallic site catalyst with a Cu-O-Ti structure, utilizing the synergistic effect of Cu and Ti to promote the electrochemical reduction of NO. The highest Faraday efficiency reached 93.7%, which is superior to the currently reported catalysts for the same reaction. At the same time, the d-π coupling brought about by the bimetallic sites further promotes the transfer of electrons. Overall, the content of the article is rich and the structure is clear. However, the presentation of some experimental evidence is not sufficient, and there are some confusing parts. Additionally, regarding certain evidence chains, we have some concerns and would suggest that the authors revisit and potentially revise these sections to strengthen their argument.*

Response: Thank you for taking the time to review our manuscript and providing us with your insightful comments. We greatly appreciate your efforts in helping us enhance the quality of our research findings. All your comments were responded to in a thorough and transparent manner, which you will find below. We firmly believe that these revisions have substantially improved the quality of our manuscript. The corresponding revisions are described as follows:

1. The bimetallic site catalyst designed by the authors achieved a very high Faraday efficiency and electrocatalytic ammonia synthesis performance, but the research on control experiments and by-products was too weak. For instance, are there any relevant data directly proving the electrocatalytic ammonia synthesis performance of structures such as Cu-O-Cu? Additionally, for the reaction using NO as the raw material, are there any other N-N bonded products, such as N_2, in the products?

Response: We thank the reviewer very much for these kind comments. Following the suggestion, we synthesized a Cu−O−Cu structure on Ti felt substrate by increasing the copper loading to 1.17 wt%, which was determined by inductively coupled plasma optical emission spectrometry (ICP-OES). The formation of the Cu−O−Cu structure was successfully verified by the distinct nanoparticles observed in HAADF-STEM images and the characteristic Raman signal of copper oxide at 290 cm^{-1} (*J. Am. Chem. Soc.* **2020**, 142, 11417–11427). As presented

in **Figure R16**, both the NH_3 yield and Faradaic efficiency of the Cu−O−Cu sample at various applied potentials were lower than those of the Cu_1−Ti pair sites.

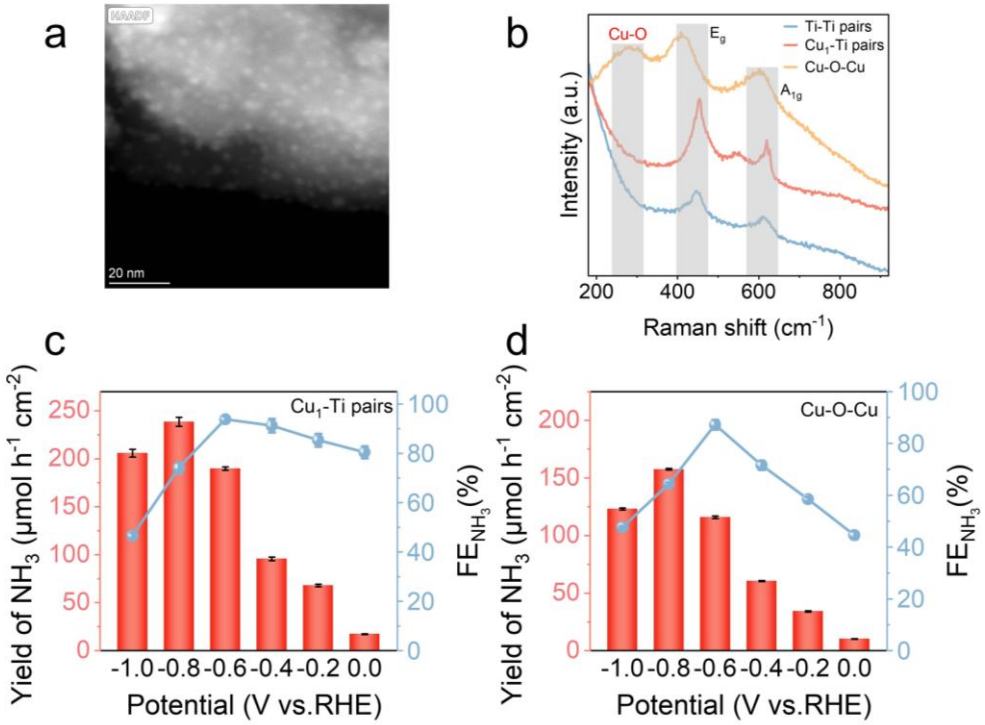

Figure R16. (a) HADDF-STEM image of Cu−O−Cu. (b) The Raman spectra of Cu−O−Cu, Ti−Ti pairs, and Cu_1−Ti pairs. NH_3 yield rates and FE_{NH3} of (c) Cu_1–Ti pairs, and (d) Cu−O−Cu.

Regarding the product selectivity of NORR, we first employed DEMS to detect the gaseous byproducts, including N_2 and N_2O. As shown in **Figure R17**, no characteristic signals corresponding to N_2 or N_2O were detected for either the Cu_1−Ti pairs or Ti−Ti pairs, suggesting that N_2 and N_2O are not generated during the NORR. Subsequently, we used colorimetric assays to quantify the liquid-phase byproducts including hydroxylamine (NH_2OH) and hydrazine (N_2H_4). The quantification of NH_2OH and N_2H_4 were performed according to Frear's method and the Watt-Chrisp method, respectively (*Nat. Synth.* **2025**, 4, 1598–1609; *Nat. Catal.* **2023**, 6, 949-958.). As shown in **Figure R18**, the highest concentration of NH_2OH was merely 0.01 μmol L^{-1} at −0.8 V vs. RHE, along with a Faradaic efficiency of 1.5%. Meanwhile, the concentration of formed N_2H_4 was below the detection limitation (5 μmol L^{-1}), suggesting the negligible generation of N_2H_4 during the NORR (**Figure R19**).

Figure R17, R18 and **R19** were added on **Page 19-21** in the revised Supporting Information as **Supplementary Figure S17, S18** and **S19**, respectively**.** And the related discussion was added on **Page 7 Line 126-130** in the revised manuscript as follows:

"At this potential, the Cu_1−Ti pairs delivered an exceptional NH_3 yield of 189.9 μmol h^{-1} cm^{-2} with a FE_{NH3} of 93.7%, significantly outperforming the Ti−Ti pairs control (58.5 μmol h^{-1} cm^{-2}, 63.5% FE_{NH3}) and most reported NORR catalysts (Figure 2f, Table S2). Besides, NH_2OH was detected as the only byproduct with a corresponding Faradaic efficiency of 1.5% (Figures S17-19)."

Besides, the detect methods for NH_2OH and N_2H_4 were respectively added on **Page 44-45** in the revised Supporting Information as **Supplementary Note 6** and **Supplementary Note 7** as follows:

"The concentration of NH_2OH was determined according to Frear's method. The standard solution was prepared by diluting the mother liquor (0.5 mM $NH_2OH{\cdot}HCl$ aqueous solution containing 0.25 M K_2SO_4). First, 1 mL of standard solution was placed in a clean centrifuge tube. Then, 1 mL of 0.1 M PBS solution, 1 mL deionized water and 0.2 mL of 12 wt% trifluoroacetic acid were added in order, followed by 1 mL of 10 g L^{-1} 8-quinolinol ethanol solution. Finally, 1 mL of 1 M Na_2CO_3 solution was added. The vials were then placed in a 60 °C oven for 15 min and cooled for another 10 min. The absorption spectrum was recorded on an UV–vis spectrophotometer in the wavelength range 600–800 nm. The solution without $NH_2OH{\cdot}HCl$ was used for background correction. The absorbances were recorded at a wavelength of 705 nm and plotted against the hydroxylamine concentrations. The test of the target sample follows the same process as the standard solution.

The N_2H_4 product in the electrolyte solution was measured by the Watt-Chrisp method. Briefly, 10 mL of HCL, 2 g of para-(dimethylamino) benzaldehyde and 100 mL of C_2H_5OH were dissolved and used as a sensitive chromogenic reagent. Then, 2 mL of solution product was collected from the cathode compartment and uniform mixed with 5 mL of the chromogenic reagent at room temperature. After standing for 20 min in the dark for at room temperature, the light absorbance of the resulting solution was detected by UV-Vis spectrophotometer at the

wavelength of 457 nm."

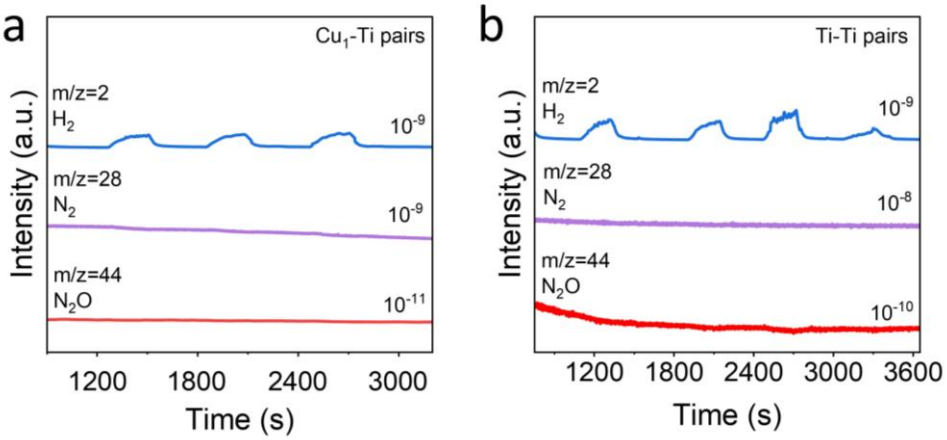

Figure R17. The signal spectrum of the intermediates on (a) Cu_1−Ti pairs and (b) Ti−Ti pairs monitored by DEMS during the NORR.

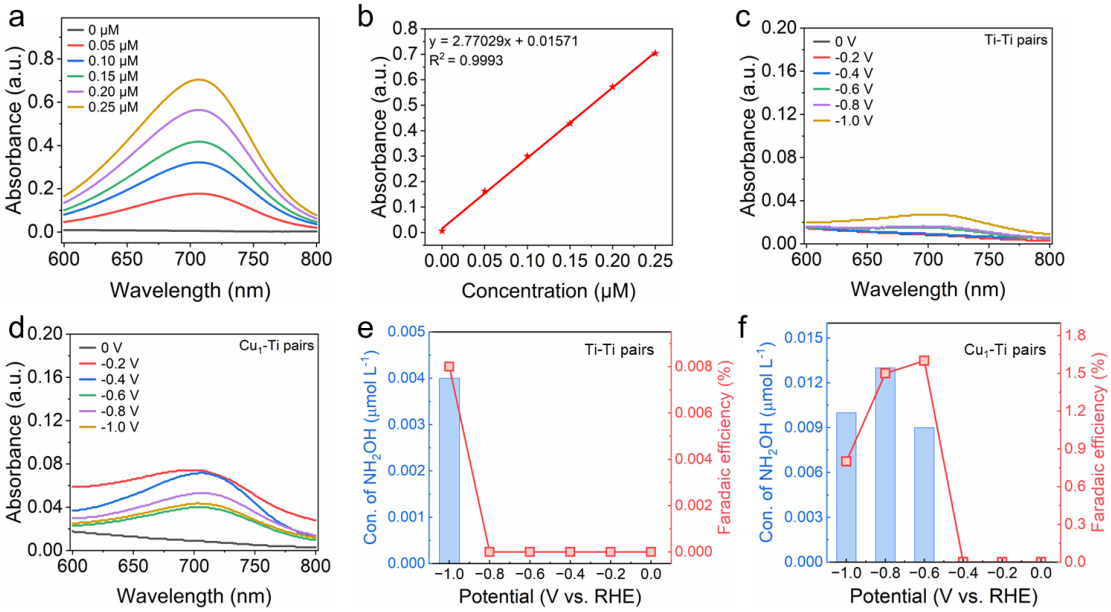

Figure R18. (a) UV-Vis absorption spectra of NH_2OH assays. (b) Calibration curve for quantitative calculation of NH_2OH concentrations. UV-Vis spectra for NH_2OH produced by (c) Ti−Ti pairs and (d) Cu_1−Ti. Corresponding NH_2OH concentration and Faradaic efficiency of (e) Ti−Ti and (f) Cu_1−Ti pairs.

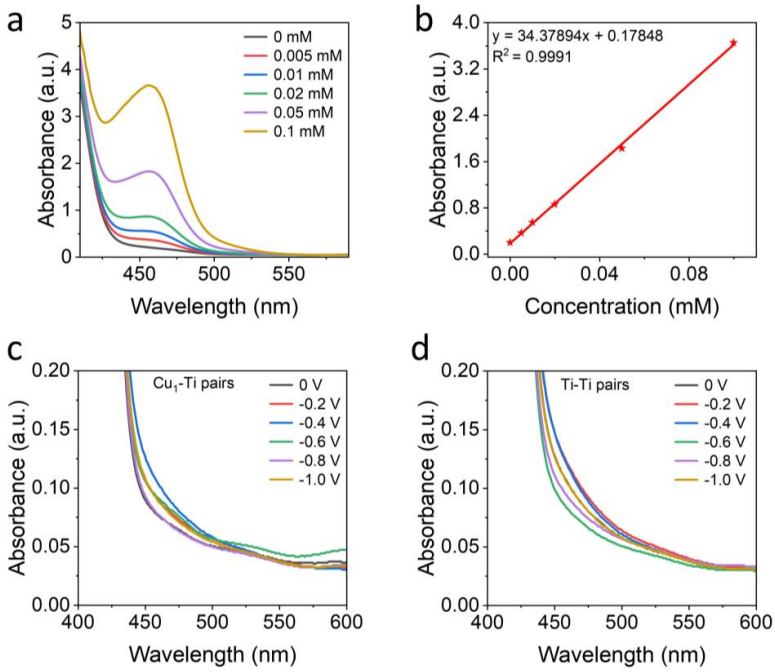

Figure R19. (a) UV-Vis absorption spectra of N_2H_4 assays. (b) Calibration curve for quantitative calculation of N_2H_4 concentrations. UV-Vis spectra for N_2H_4 produced by (c) Cu_1−Ti pairs and (d) Ti−Ti pairs.

2. Although HAADF-STEM and EXAFS data support the single-atom dispersion of Cu, the precise coordination structure and formation ratio of the Cu_1-Ti heteronuclear bidentate pair have not yet been confirmed. The fitting path of the Cu-Ti scattering peak at 2.58 Å in EXAFS is not unique, and no synchrotron radiation data of the Ti K-edge is provided to verify the change in the coordination environment of Ti. Considering that there are various defect sites on the TiO_2 surface, the current data cannot rule out the possibility that the Cu atoms are randomly distributed in different oxygen vacancies rather than forming a unified active pair. This structural uncertainty directly affects the credibility of the mechanism explanation.

2.1 Although HAADF-STEM and EXAFS data support the single-atom dispersion of Cu, the precise coordination structure and formation ratio of the Cu_1-Ti heteronuclear bidentate pair have not yet been confirmed. The fitting path of the Cu-Ti scattering peak at 2.58 Å in EXAFS is not unique, and no synchrotron radiation data of the Ti K-edge is provided to verify the change in the coordination environment of Ti.

Response: We thank the reviewer very much for these insightful comments. In the revision,

we provide more detailed discussions to clarify the coordination environment of Cu_1−Ti pairs as follows:

First, we would like to clarify the meaning of the EXAFS *R*-space data. *R* space is the radial distribution function obtained by Fourier transforming $\chi(k)$ from *k* space, which can directly reflect the average radial distances between the absorbing atom and coordinating atoms. We carefully compared the R space spectra of Cu_1–Ti with those of the standard Cu_2O and CuO. Our analysis of *R* space demonstrated that the second coordination shell peak position (i.e., 2.58 Å for Cu_1−Ti) differed from Cu−O−Cu signatures in both Cu_2O (2.70 Å) and CuO (2.49 Å), thereby excluding its assignment to Cu−O−Cu configurations (**Figure R20a**). Moreover, the peak at 2.58 Å were attributed to the Cu−Ti coordination, which has also been reported in the prior literature (*Nano Energy.* **2022**, 103, 107853; *Nat Commun.* **2023**, 14, 1117; *Nat Commun.* **2025**, 16, 665). The *R* factors, which present the fractional difference between experimental and theoretical EXAFS functions over the experimental EXAFS, were 0.0114 for Cu_1−Ti, demonstrating the fitting validness.

During this revision, we also supplemented Ti K-edge XAFS to verify the change in the Ti coordination environment. As shown in **Figure R20b-c**, the Ti–O coordination in the Cu_1–Ti pairs sample is considerably stronger than that in the Ti felt. These results suggested that OVs on Ti substrate served as anchoring sites for isolated Cu atoms, matched well with the results of EPR showing a obvious declined OVs signals of Cu_1–Ti pairs compared with that of Ti felt and Ti-Ti pairs (**Figure R20d**). Meanwhile, we observed an enhanced intensity in the second coordination shell of Ti atoms, likely induced by the incorporation of Cu single atoms. However, distinguishing Ti–O–Cu from Ti–O–Ti coordination remains challenging owing to the extremely low Cu loading (0.38 wt%) and the strong interference from the dominant Ti–O–Ti framework.

Figure R20b-d was added on **Page 5** in the revised Supporting Information as **Supplementary Figure S4**.

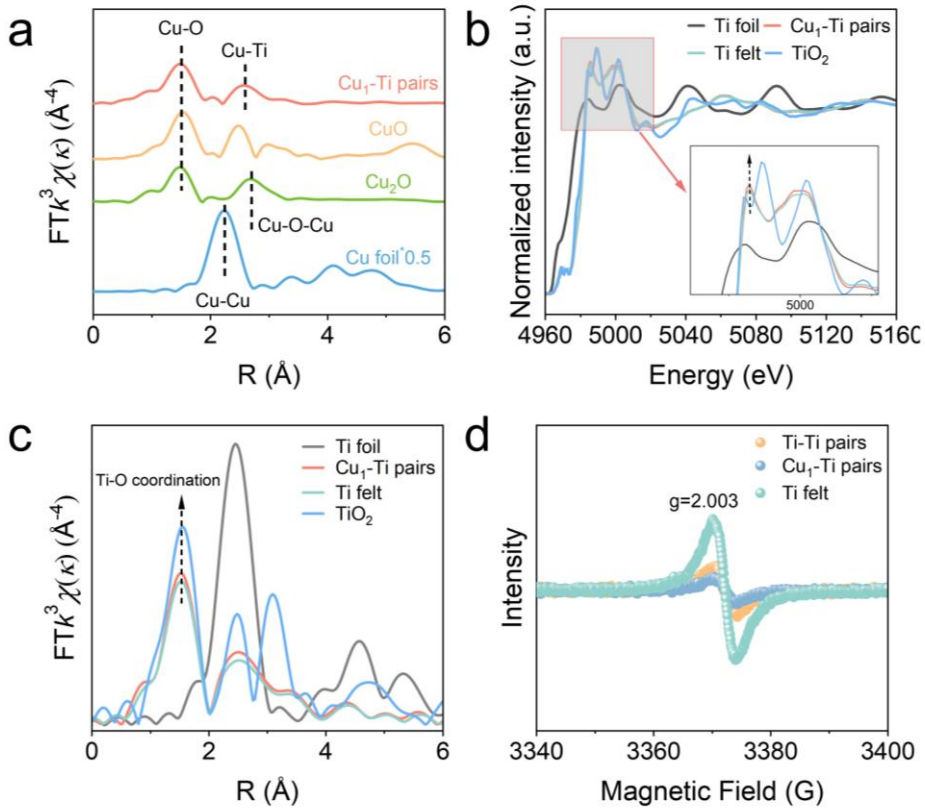

Figure R20. (a) FT EXAFS spectra of Cu_1−Ti pairs, CuO, Cu_2O, and Cu foil at the Cu K-edge. (b) XANES spectra and (c) FT EXAFS spectra of Ti foil, Cu_1−Ti pairs, Ti felt, and TiO_2 at the Ti K-edge. (d) EPR spectra of Ti felt, Ti−Ti pairs, and Cu_1−Ti pairs.

2.2 Considering that there are various defect sites on the TiO_2 surface, the current data cannot rule out the possibility that the Cu atoms are randomly distributed in different oxygen vacancies rather than forming a unified active pair. This structural uncertainty directly affects the credibility of the mechanism explanation.

Response: We acknowledge that TiO_2 surfaces inherently possess various defect sites, and it is indeed challenging to achieve an absolutely uniform distribution of active sites in heterogeneous catalytic systems. From an atomic-level perspective, the dominant configurations on the Ti felt after oxygen vacancy (OVs) formation were Ti–OV–Ti motifs. In this work, our focus was not on the specific type of oxygen vacancies, but rather on the atomic-scale Ti–OV–Ti configurations, which served as the preferential anchoring sites for Cu single atoms to form heteronuclear Cu_1−Ti catalytic pairs, regardless of the OVs type. In this case,

the Cu_1−Ti pairs will drive NORR via a bidirectional electron donation mechanism.

3. Since the authors have already elaborated on the practical application scenarios of exhaust gas treatment in the background section, in the article, evidence should be used to support the corresponding viewpoints. We do not deny the excellent performance of the catalyst designed by the authors. However, the raw material used is a mixture of 20% NO and 80% Ar. The proportion of NO in this mixture is too high. Could the authors consider conducting relevant experiments in an environment with a low concentration of NO to further highlight the key points of the article? Especially when comparing the content of this article with the currently reported catalysts, we can see obvious performance differences under more demanding conditions. However, the current data fails to highlight the advantages of the bimetallic catalyst.

Response: We thank the reviewer very much for these insightful comments and suggestions. As suggested, we conducted electrochemical NORR experiments under a low NO concentration (1 vol% NO/Ar). This concentration was chosen based on previous literatures *(Nat. Commun.* **2025**, 16, 8481; *Adv. Mater.* **2025**, 37, 2504497; *ACS Nano* **2026**, 20, 2323–2336). Under this low NO concentration, the Cu_1−Ti pairs achieved a maximum Faradaic efficiency of 89.1% at −0.6 V vs. RHE and an NH_3 production rate of 37.59 μmol h^{-1} cm^{-2}, which was significantly superior to most reported electrocatalysts (**Figure R21**). These results highlight the advantages of bimetallic Cu_1−Ti pairs for nitric oxide electroreduction to ammonia through the bidirectional electron donation mechanism.

Figure R21 was added on **Page 22** in the revised Supporting Information as **Supplementary Figure S20** and the related discussion was added on **Page 7-8 Line 130-133** in the revised manuscript as follows:

"To enhance practical applicability, we also conducted NORR tests under a low NO concentration (1 vol% NO/Ar). Notably, the Cu_1−Ti pairs achieved an optimized NH_3 production rate of 37.59 μmol h^{-1} cm^{-2} and FE of 89.1%, which is superior to most reported electrocatalysts under identical conditions (Figure S20)."

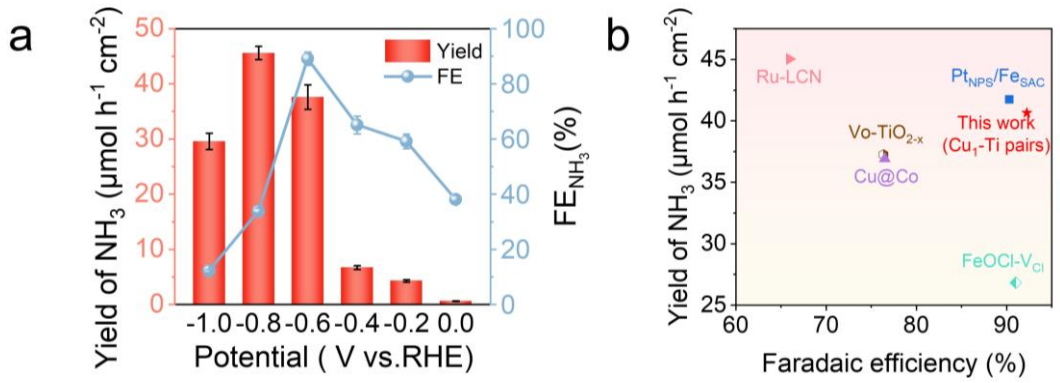

Figure R21. (a) NH_3 yield rates and FE_{NH3} of Cu_1–Ti pairs in 1 vol% NO-saturated 0.25 M K_2SO_4. (b) Comparisons of the NORR performance of Cu_1–Ti pairs with other previously reported electrocatalysts under 1 vol% NO/Ar.

*4. The improvements made in the manuscript regarding the activation mechanism of N=O based on the orbital theory are extremely fascinating. However, the rigor of some of the data may need to be further improved. For instance, in Fig 3e, the assignment of *NO (side-on) is rather arbitrary and lacks rigorous validation such as isotope labeling. This significantly undermines the theoretical explanations for "side-on adsorption" and "end-on adsorption". In addition, regarding the tests of the experimental results, we suggest that the authors should carefully consider the interference of K^+ ions in the electrolyte, surface hydroxyl groups, or other nitrogen-containing species.*

*4.1 The improvements made in the manuscript regarding the activation mechanism of N=O based on the orbital theory are extremely fascinating. However, the rigor of some of the data may need to be further improved. For instance, in Fig 3e, the assignment of *NO (side-on) is rather arbitrary and lacks rigorous validation such as isotope labeling. This significantly undermines the theoretical explanations for "side-on adsorption" and "end-on adsorption".*

Response: We thank the reviewer very much for these insightful comments and suggestions. We agree that isotope labeling experiments are a powerful tool for accurately assigning vibrational modes and enhancing the reliability of our findings.

Theoretically, the peak position and intensity of infrared spectroscopy can be basically explained by the harmonic oscillator model, and the two are closely related: chemical bonds in molecules can be approximated as classical harmonic oscillators, whose vibration frequency is determined by the force constant of the bond and the reduced mass of the vibrating atoms. This relationship is the core theoretical basis for infrared spectrum analysis. Within the framework of classical mechanics, the vibration frequency ν follows the equation 1:

$$\nu = \frac{1}{2\pi}\sqrt{\frac{k}{\mu}} \qquad \text{(Equation 1)}$$

Where k is the bond force constant, and $\mu = m_1m_2/(m_1+m_2)$ is the reduced mass.

The corresponding wavenumber expression is:

$$\sigma = \frac{1}{2\pi c}\sqrt{\frac{k}{\mu}} \approx 1307\sqrt{\frac{k}{\mu}} \qquad \text{(Equation 2)}$$

For the adsorption system of NO molecules, when NO is adsorbed on the catalyst surface in a side-on or end-on configuration, the force constant (k) of the N-O bond will change; at the same time, isotope labeling (such as substituting ^{15}NO for ^{14}NO) will change the reduced mass (μ) of the vibrating atoms. According to the harmonic oscillator model, both will lead to a characteristic shift of the infrared absorption peak—which is also the core principle for distinguishing NO adsorption configurations and confirming adsorption sites through isotope infrared spectroscopy.

The ratio (γ) of the infrared frequency downward in N^{15}O could be approximately analyzed by following equation 3:

$$\gamma = \frac{\nu(N^{15}O)}{\nu(N^{14}O)} = \frac{\sqrt{m(N^{15})+m(O^{16})}}{\sqrt{m(N^{15})\times m(O^{16})}} \Big/ \frac{\sqrt{m(N^{14})+m(O^{16})}}{\sqrt{m(N^{14})\times m(O^{16})}} = n\,\frac{\frac{\sqrt{15+16}}{\sqrt{15\times16}}}{\frac{\sqrt{14+16}}{\sqrt{14\times16}}} = 98.21\% \qquad \text{(Equation 3)}$$

During this revision, we have supplemented ^{15}N-labeled NO in situ electrochemical attenuated total reflection infrared spectroscopy (ATR-IRAS) to more rigorously validate the assignment of *NO adsorption configuration and other nitrogen-containing species. As shown in **Figure R22**, the peak near 1577 cm^{-1} for Cu$_1$–Ti shifts to a lower wavenumber of approximately 1548 cm^{-1} under a ^{15}NO atmosphere, whereas the peak for Ti–Ti shifts from

1737 cm^{-1} to 1712 cm^{-1}. Therefore, the peaks of *NO around 1548 cm^{-1} at Cu_1-Ti and 1712 cm^{-1} at Ti−Ti pairs surface in ^{15}NO experiment matched well with the theoretical value (1577 cm^{-1} × 98.21% = 1549 cm^{-1} for Cu_1-Ti; 1737 cm^{-1} × 98.21% = 1706 cm^{-1} for Ti−Ti pairs). These isotopic shifts unambiguously assigned the peaks at 1577 cm^{-1} and 1737 cm^{-1} to a side-on and end-on NO adsorption mode.

For other nitrogen-containing intermediates, only the *NHO species exhibited a pronounced isotope-induced redshift, as rationalized by the difference in reduced mass. For the N–H related band, the calculated isotopic frequency ratio $\gamma_{(N\text{-}H)}$ was 99.78%, higher than that for N–O $\gamma_{(N\text{-}O)}$ (98.21%). In this case, the peaks for $*NH_2$ (1507 cm^{-1}), NH_3 (1457 cm^{-1}) and $*NH_2OH$ (1181 cm^{-1}) would shift to 1504, 1543 and 1176 cm^{-1}, respectively. The redshift value was less than 4 cm^{-1}, close to the resolution limit of the ATR-IRAS spectrometer. Consequently, the isotopic shifts of these species are less obvious compared with those of NO or *NHO.

$$\gamma_{(N\text{-}H)} = \frac{\nu(N^{15}H)}{\nu(N^{14}H)} = \frac{\sqrt{m(N^{15})+m(H^1)}}{\sqrt{m(N^{15})\times m(H^1)}} \Big/ \frac{\sqrt{m(N^{14})+m(H^1)}}{\sqrt{m(N^{14})\times m(H^1)}} = \frac{\sqrt{\frac{15+1}{15\times 1}}}{\sqrt{\frac{14+1}{14\times 1}}} = 99.78\% \qquad \text{(Equation 4)}$$

Figure R22 was added on **Page 25** in the revised manuscript as **Figure 3c-d** and the related discussion was added on **Pages 10-11 Line 184-203** in the revised manuscript as follows:

"*In situ* electrochemical attenuated total reflection infrared spectroscopy (ATR-IRAS) was performed identify adsorbed intermediates and clarify the reaction mechanism. Under applied potentials in a NO-saturated electrolyte, Ti−Ti pairs exhibited a weak adsorption peak at 1737 cm^{-1}, assigned to the end-on adsorbed NO.[46, 47] Moreover, the potential-dependent evolution of intermediates (Figure 3c-d) revealed characteristic bands for *NHO (1540, 1560 cm^{-1}),[2, 46] $*NH_2OH$ (1181 cm^{-1}),[21, 47, 48, 49, 50] $*NH_2$ (1507 cm^{-1}),[21, 47, 51] and NH_3 (1457 cm^{-1}).[20, 21, 50] We proposed that NH_3 formation on both Ti−Ti and Cu_1−Ti pairs proceeds via the pathway: NO → *NHO → *NHOH → $*NH_2OH$ → $*NH_2$ → NH_3.

The isotope labeling experiments using ^{15}NO was conducted to further confirm the NO adsorption configurations and reaction intermediates. Upon substituting the ^{14}NO with ^{15}NO, the peak at 1737 cm^{-1} appeared a pronounced redshift to 1712 cm^{-1}, close to the theoretically

predicted N−O stretching frequency at 1706 cm^{-1}, based on the reduced mass in a simple harmonic oscillator model. Meanwhile, the *NHO peaks also exhibited two prominent isotopic redshifts of 16 cm^{-1} and 28 cm^{-1}, whereas shifts for other N-containing intermediates were indistinct, owing to the small frequency ratio ($\nu^{15}N/\nu^{14}N \approx 99.78\%$). Notably, Cu_1−Ti pairs displayed a side-on NO adsorption peak at 1577 cm^{-1}, which redshifted to 1548 cm^{-1} under the feedstock of ^{15}NO. The switching of NO adsorption from end-on to side-on configuration on Cu_1−Ti pairs, in agreement with our theoretical predictions, provided a dual-electron transfer channel for more effective *NO activation. Collectively, the complementary results from *in situ* Raman and isotope-labeled ATR-IRAS provide direct and consistent evidence for the proposed side-on Ti–N=O–Cu adsorption geometry under NORR reaction conditions (Figure 3e)."

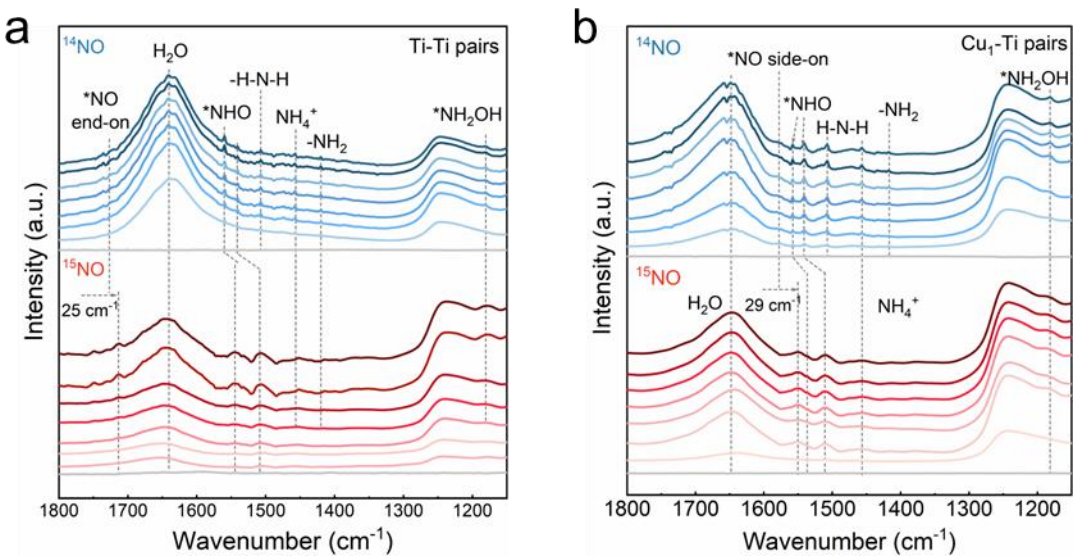

Figure R22. *In situ* ATR-IRAS spectra of adsorbed NO species and intermediates using ^{14}NO and ^{15}NO isotopic labeling on (a) Ti–Ti pairs and (b) Cu_1−Ti pairs, collected at potentials stepped from open circuit potential to −0.6 V with an interval of −0.1 V.

4.2 In addition, regarding the tests of the experimental results, we suggest that the authors should carefully consider the interference of K^+ ions in the electrolyte, surface hydroxyl groups, or other nitrogen-containing species.

Response: Regarding the concern about the interference of K^+ ions in the electrolyte, surface hydroxyl groups, or other nitrogen-containing species. To eliminate the possible interference

of K^+ ions on the ATR-IRAS spectra, we conducted control experiment by replacing the K_2SO_4 electrolyte with Na_2SO_4. As shown in **Figure R23**, the peaks assigned to NO, NHO and other intermediates remained unchanged, suggesting that the interference of K^+ ions on the interpretation of ATR-IRAS spectra was negligible. In addition to the direct experimental evidence, the characteristic wavenumbers for NORR analysis fall within the range of 1800 ~ 1150 cm^{-1}. In contrast, the characteristic signals corresponding to K^+ ions and surface hydroxyl groups typically appear in the range of 3000-3700 cm^{-1} (*Angew. Chem. Int. Ed.* **2026**, 65, e21249; *Adv. Energy Mater.* **2026**, e70813; *Nat Catal.* **2022**, 5, 900–911; *Adv. Funct. Mater.* **2025**, e26511.), further confirming that K^+ ions and surface hydroxyl groups did not interfere with the NORR-related spectral analysis.

Regarding other nitrogen-containing species, the characteristic peaks of the relevant intermediates were clearly distinguished and reasonably assigned based on previous reports (**Table R3**), which guaranteed the reliability and accuracy of our spectral identification and data analysis.

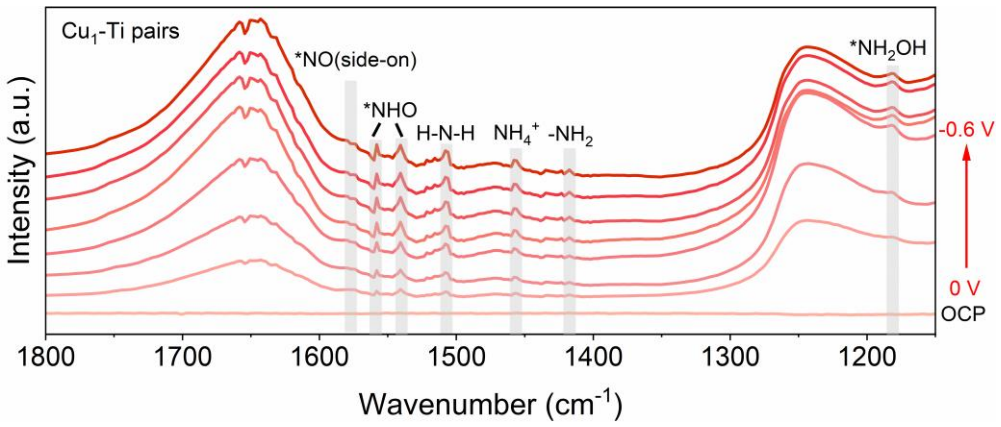

Figure R23. *In situ* ATR-IRAS spectra of Cu_1−Ti pairs during the NORR in 0.25 M Na_2SO_4.

Wavenumber (cm^{-1})	Species	Ref.
1190	*NH_2OH	*ACS Energy Lett.* **2023**, 8, 1281-1288. *J. Mater. Chem. A.* **2024**, 12, 15651-15657. *Angew. Chem., Int. Ed.* **2025**, e202504499. *Nano Lett.* **2024**, 24, 541-548. *ACS Catal.* **2023**, 13, 9550-9557.
1457	H–N–H	*ACS Energy Lett.* **2023**, 8, 1281-1288. *J. Mater. Chem. A.* **2024**, 12, 15651-15657. *Nat. Commun.* **2025**, 16, 4874.
1507	NH_4^+	*Angew. Chem., Int. Ed.* **2024**, 136, e202318792. *ACS Energy Lett.* **2023**, 8, 1281-1288. *ACS Catal.* **2023**, 13, 9550-9557.
1540	*NHO	*Angew. Chem., Int. Ed.* **2025**, 64, e202420346.
1560	*NHO	*Angew. Chem., Int. Ed.* **2023**, 135, e202305184.
1577	*NO side-on	*Proc. Natl. Acad. Sci.* **2024**, 121, e2405236121.
1737	*NO end-on	*J. Mater. Chem. A.* **2024**, *12, 15651–15657* *Angew. Chem. Int. Ed.* **2023**, 62, e202305184

Table R3. The wavenumbers of the absorption bands and the corresponding intermediates in the IR spectra based on the reported literatures.

5. The authors should carefully review all the details in the text. Some of the errors are quite detrimental to the readers' reading and comprehension. For example, the expression of uniformly occupied oxygen vacancies (Ovs and OVs); Regarding the correspondence of each figure in Fig 3 with the content of the article, as well as the explanation of the specific meaning of the symbol "|e|" that appears in the article and the relevant literature references.

Response: Thanks very much for the reviewer's kind reminder. During this reversion, we carefully recheck and standardized the expression of occupied oxygen vacancies as OVs to ensure uniformity throughout the text. Moreover, we have revised the description of **Figure 3** and improved the correspondence between each panel and the related content in the article.

The meaning of the symbol "|e|": We calculated the atomic charge based on Bader charge analysis,[1, 2, 3] which has been proven to be the most intuitive descriptors of charge distribution in chemical systems, to investigate the charge transfer in catalytic process.[4, 5, 6] And in the context of Bader charge analysis, |e| denotes the absolute value of the elementary charge, used here to indicate the number of electrons transferred (in units of e^-). The net charge on an atom q(Ω), is given by the sum of its nuclear charge $Z_\Omega e$ and its average electronic charge -N(Ω)e

$$q(\Omega)=(Z_\Omega-N(\Omega))e.$$

When one is concerned with the magnitude of the change in atomic charge relative to the neutral atom, it can also be calculated using the following formula:

$$|q(\Omega)|=|Z_\Omega-N(\Omega)||e|$$

6. The title of this manuscript was: "Bidirectional electron donation in heteronuclear catalytic pairs for efficient nitric oxide electroreduction to ammonia". We think the title is too broad and overstated, implying that similar all catalysts are suitable without any specificity.

Response: We thank the reviewer very much for these kind comments. According to the reviewer`s suggestion, we revised the title of manuscript into "Bidirectional electron donation in heteronuclear Cu_1−Ti pairs for efficient nitric oxide electroreduction to ammonia".

Reviewer #5 (Remarks to the Author):

This work reports a heteronuclear Cu_1−Ti dual-atom catalyst for efficient electrocatalytic NO reduction to NH3, leveraging complementary N/O affinities of Ti/Cu to achieve side-on adsorption and bidirectional electron transfer. The integration of experimental characterizations (e.g., in situ ATR-IRAS, DEMS) and DFT calculations is rigorous, and the catalyst exhibits impressive FE (93.7%) and NH_3 yield. Overall, I recommend its publication after minor revisions. Some specific comments are provided as follows.

Response: Thank you for taking the time to carefully review our manuscript and provide extensive feedback. According to your suggestions, we have conducted additional experiments and included detailed point-by-point responses to your comments. The corresponding revisions are described as follows:

1. The formation mechanism of Cu_1−Ti pairs mentions oxygen vacancies (OVs) but lacks atomic-level details on how Cu precisely embeds into Ti−Ov−Ti motifs. Please supplement structural evolution evidence (e.g., ex situ XAFS at different annealing stages).

Response: We thank the reviewer for this insightful comment regarding the atomic-level formation mechanism of Cu_1−Ti pairs. We agree that elucidating how Cu atoms are precisely incorporated into the Ti−OV−Ti framework is essential for validating our catalyst design strategy. Accordingly, we performed comprehensive characterizations to provide the structural evolution evidence including EPR spectra, *ex situ* Cu K-edge XAFS and Ti K-edge XAFS.

As shown in EPR spectra **(Figure R24a)**, the surface on the pristine Ti felt was enriched with OVs. After heat treatment, the concentration of OVs on the surface of Ti–Ti pairs decreased, and further declined after the formation of Cu_1–Ti pairs, indicating that Cu atoms occupied the OVs sites.

We further performed *ex situ* Cu K-edge XAFS to trace the coordination environment evolution of Cu during the synthesis of Cu_1–Ti pairs. The tested samples included the $CuCl_2$ precursor, the intermediate sample annealed for 0.5 h (donated as Cu_1–Ti pairs-0.5 h) and the

final catalyst annealed for 3 h (Cu_1–Ti pairs). As shown in **Figure R24b-c**, the dominated peak for $CuCl_2$ precursor was at 1.90 Å, ascribing to the Cu–Cl coordination. In contrast, the peak for Cu_1–Ti pairs-0.5 h shifted to 1.47 Å, corresponding to the Cu–O coordination. Combined with results of EPR and *ex situ* Cu K-edge XAFS, we believed that Cu atoms migrated into OV sites and transformed from Cu–Cl to Cu–O coordination.

With increasing annealing time from 0.5 h to 3 h under an oxygen-containing atmosphere, the Cu–O coordination was further intensified, and the Cu–Ti scattering peak in the second shell was significantly enhanced. This observation can be rationalized by the incorporation of oxygen atoms from O_2 molecules, which bridge Cu and adjacent Ti atoms at elevated temperatures, promoting the formation of stable Cu_1–Ti local structures (*J. Am. Chem. Soc.* **2023**, 145, 2523–2531). Meanwhile, *ex situ* Ti K-edge XAFS results (**Figure R24d-e**) further corroborated these findings. The Ti–O coordination as well as the Ti-O-Ti/Cu scattering feature in the Cu_1–Ti pairs is considerably stronger than that in the pristine Ti felt.

Combined the results from EPR and *ex situ* Ti/Cu K-edge XAFS, we could conclude that the formation mechanism that Cu^{2+} are initially trapped by OV sites, lose their Cl ligands to bond with O atoms, and then gradually interact with adjacent Ti atoms to form stable Cu_1–Ti pairs as annealing proceeds.

During this revision, **Figure R24** was added on **Page 5** in the revised Supporting Information as **Supplementary Figure S4** and the related discussion was added on **Page 5-6 Line 30-50** in the revised Supporting Information as follows:

"To elucidate the formation mechanism, we performed EPR spectra, ex situ Ti K-edge XAFS and Cu K-edge XAFS. As shown in EPR spectra (Figure S4a), the surface on the pristine Ti felt was enriched with OVs. After heat treatment, the concentration of OVs on the surface of Ti–Ti pairs decreased, and further declined after the formation of Cu_1–Ti pairs, indicating that Cu atoms occupy the OVs sites.

We further performed ex situ Cu K-edge XAFS to trace the coordination environment evolution of Cu during the synthesis of Cu_1–Ti pairs (Figure S4b). The tested samples included the $CuCl_2$ precursor, the intermediate sample annealed for 0.5 h (donated as Cu_1–Ti pairs-0.5

h) and the final catalyst annealed for 3 h (Cu_1–Ti pairs). As shown in Figure S4c, the dominated peak for $CuCl_2$ precursor was at 1.90 Å, ascribing to the Cu–Cl coordination. In contrast, the peak for Cu_1–Ti pairs-0.5 h shifted to 1.47 Å, corresponding to the Cu–O coordination. Combined with results of EPR and ex situ Cu K-edge XAFS, we believed that Cu atoms migrated into OV sites and transformed from Cu–Cl to Cu–O coordination.

With increasing annealing time from 0.5 h to 3 h under an oxygen-containing atmosphere, the Cu–O coordination was further intensified, and the Cu–Ti scattering peak in the second shell was significantly enhanced. This observation can be rationalized by the incorporation of oxygen atoms from O_2 molecules, which bridge Cu and adjacent Ti atoms at elevated temperatures, promoting the formation of stable Cu_1–Ti local structures. Meanwhile, ex situ Ti K-edge XAFS results (Figure S4d-e) further corroborated these findings. The Ti–O coordination as well as the Ti-O-Ti/Cu scattering feature in the Cu_1–Ti pairs is considerably stronger than that in the pristine Ti felt.

Combined the results from EPR and ex situ Ti/Cu K-edge XAFS, we could conclude that the formation mechanism that Cu^{2+} are initially trapped by OV sites, lose their Cl ligands to bond with O atoms, and then gradually interact with adjacent Ti atoms to form stable Cu_1–Ti pairs as annealing proceeds."

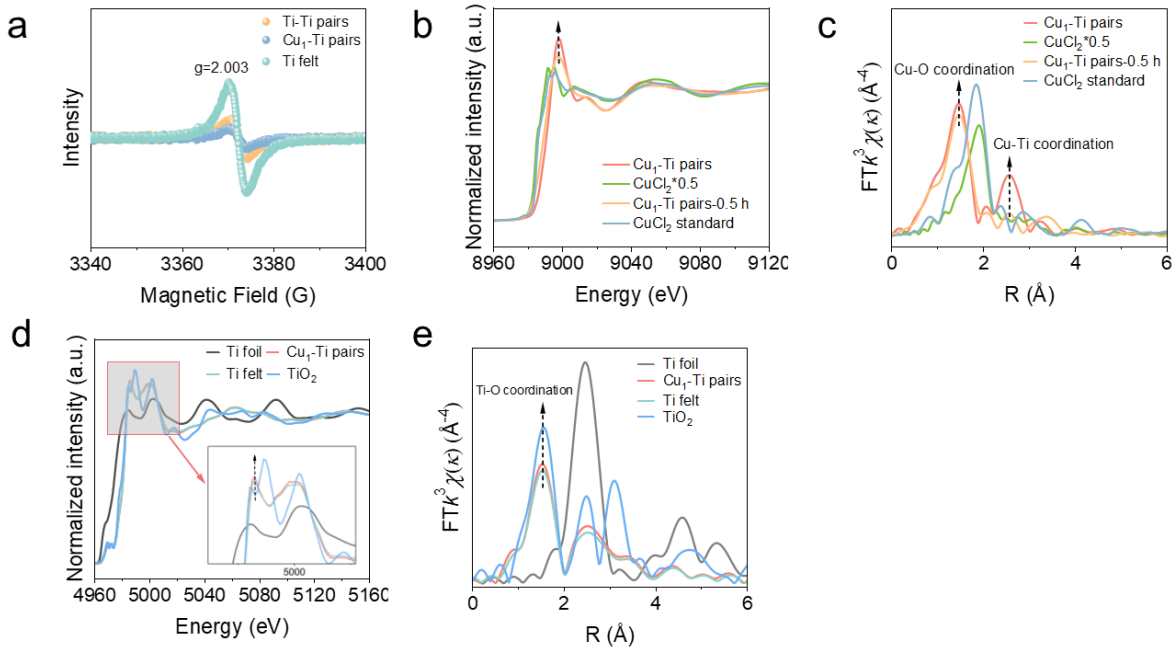

Figure R24. (a) EPR spectra of Ti felt, Ti−Ti pairs, and Cu_1−Ti pairs. The OVs exist on the surface of Ti felt. (b) XANES spectra and (c) FT EXAFS spectra of Cu_1−Ti pairs, $CuCl_2$, Cu_1−Ti pairs-0.5 h, and $CuCl_2$ reference sample at the Cu K-edge. (d) XANES spectra and (e) FT EXAFS spectra of Ti foil, Cu_1−Ti pairs, Ti felt, and TiO_2 at the Ti K-edge.

2. In Fig. 2f, comparisons with reported catalysts do not specify whether test conditions (e.g., NO concentration, electrolyte type) are consistent. Standardize parameters for fairer performance benchmarking.

Response: We thank the reviewer very much for these kind comments. As suggested, to ensure fairer performance benchmarking with reported NORR electrocatalysts in **Figure 2d**, we have clearly specified the key test parameters (including NO concentration) for all compared catalysts in the **Figure 2d** legend and **Supplementary Table S2**.

During this revision, **Figure R25** was added on **Page 24** in the revised manuscript as **Figure 2d**.

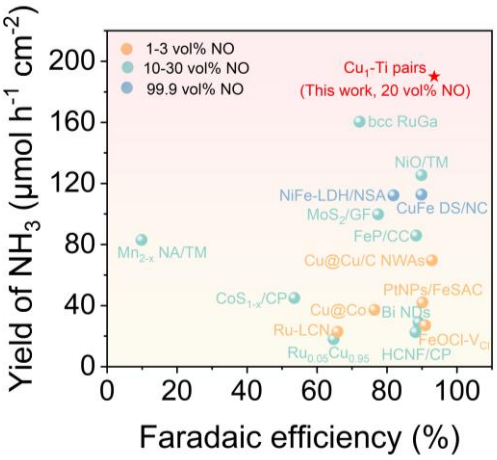

Figure R25. Comparisons of the NORR performance of Cu_1−Ti pairs with other previously reported electrocatalysts.

3. DFT calculations use a TiO_2 surface model, but the specific crystal phase (anatase/rutile) is unspecified. Clarify this as it significantly affects adsorption energy and reaction pathways.

Response: We thank the referee for this comment and suggestion. In this manuscript, the DFT calculations were performed on a rutile TiO_2 surface due to its energetic advantage. To gain a deeper understanding of the effect of Cu_1−Ti pairs, we also investigated the NO reduction coordinate on an anatase TiO_2 surface. The results show that, even on a different crystal phase, NO adsorbs in a monodentate configuration via N atom on homonuclear Ti−Ti pairs, whereas heteronuclear Cu_1−Ti pairs favor a bidentate adsorption geometry, consistent with the situation on rutile TiO_2 (**Figure R26**). For the most important step in NO reduction reaction, namely the activation of polar NO molecule, *NHO is thermodynamically favored over *NOH by 1.14 eV on Ti–Ti pairs and by 1.68 eV on Cu_1–Ti pairs, indicating that the change in crystal phase does not alter the reaction coordinate of NO reduction. Crucially, the thermodynamic barrier for this pivotal first hydrogenation step shifts from an endergonic +1.07 eV on Ti−Ti pairs to a strongly exergonic −0.88 eV on Cu_1−Ti pairs, demonstrating that the heteronuclear Cu−Ti motif provides a more effective pathway for NO activation and subsequent conversion as discussed in our research.

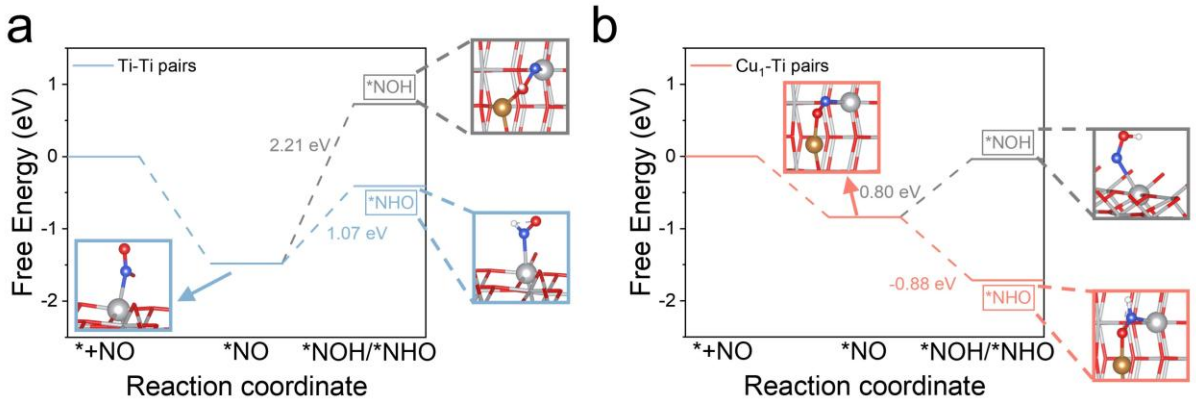

Figure R26. Calculated free energy diagrams for NO activation on (a) Ti−Ti pairs and (b) Cu_1−Ti pairs using an anatase TiO_2 surface.

4. More recently reported literatures related to this work can be properly cited to make this paper state-of-the-art: Nat. Commun., 2025, 16, 8837. Adv. Mater., 2024, 36, 2402160.

Response: Thanks for your valuable suggestion. In this revision, we have cited the related references in the manuscript as follows:

Ref. 6. Nat Commun 16, 8837 (2025).

Ref. 27. Adv. Mater. 36, 2402160 (2024).

5. Stability testing only includes 20 cycles. Provide long-term electrolysis data (e.g., 100 h) and post-reaction structural characterizations to verify resistance to agglomeration/ deactivation.

Response: We thank the reviewer very much for these kind comments. In this revision, we extended the long-term stability test to 120 h at −0.6 V vs. RHE in 0.25 M K_2SO_4 electrolyte. As shown in **Figure R27**, both the current density and FE_{NH3} remained stable without obvious decay over 120 h of continuous electrolysis. Furthermore, post-reaction characterizations verified the excellent structural stability of the Cu_1−Ti pairs. No obvious agglomeration into clusters or nanoparticles was observed in the AC-HAADF-STEM image, and the EXAFS spectrum confirmed the absence of metallic Cu–Cu scattering peaks, demonstrating high

resistance to agglomeration and deactivation (**Figure R28**).

Figure R27 and **Figure R28** were respectively added on **Pages 26** and **28** in the revised Supporting Information as **Supplementary Figure S24** and **Page 26;** and the related discussion was added on **Page 8 Line 144-146** in the revised manuscript as follows:

"Furthermore, the Cu_1−Ti pairs exhibited outstanding stability and there was no significant decrease in NH_3 yield nor FE_{NH3} during 20 consecutive electrolysis cycles (Figure 2g) and 120 h continuous NORR tests (Figure S24)."

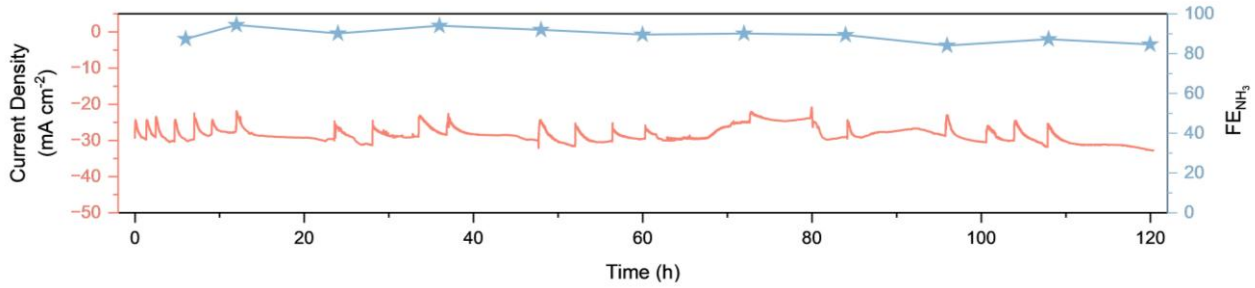

Figure R27. Long-term chronoamperometry test of Cu_1–Ti pairs at −0.6 V vs. RHE.

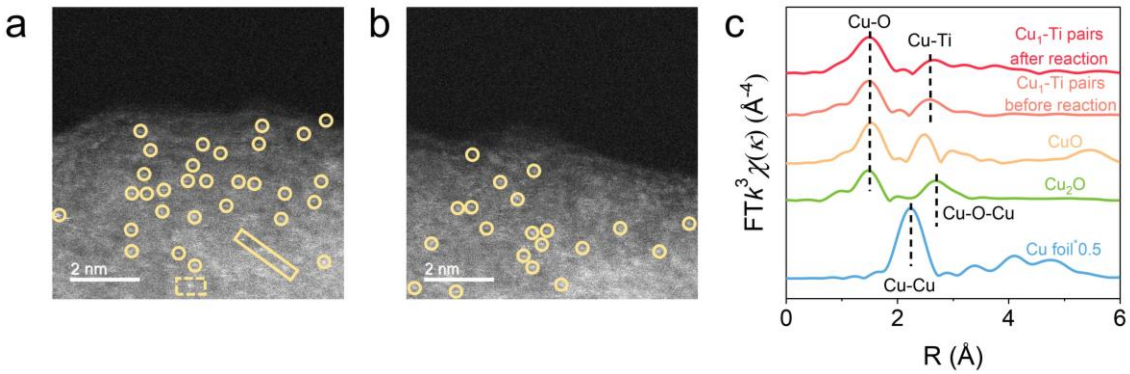

Figure R28. The HAADF-STEM images of the Cu_1−Ti pairs (a) before testing and (b) after testing. (c) FT EXAFS spectra at the Cu K-edge for Cu_1–Ti pairs before and after the reaction.

*6. The *NHO → *NH_2OH step in the reaction pathway lacks DFT-calculated free energy changes. Supplement this data to clarify its thermodynamic feasibility.*

Response: Thanks for your valuable suggestion. In this manuscript, NH_3 formation on both Ti−Ti and Cu_1−Ti pairs proceeds via the pathway: NO → *NHO → *NHOH → *NH_2OH → *NH_2 → NH_3, and we provided DFT-calculated free energy changes of the overall reaction

pathway (**Figure R29**).

Figure R29 was added on **Page 38** in the revised Supporting Information as **Supplementary Figure S36**.

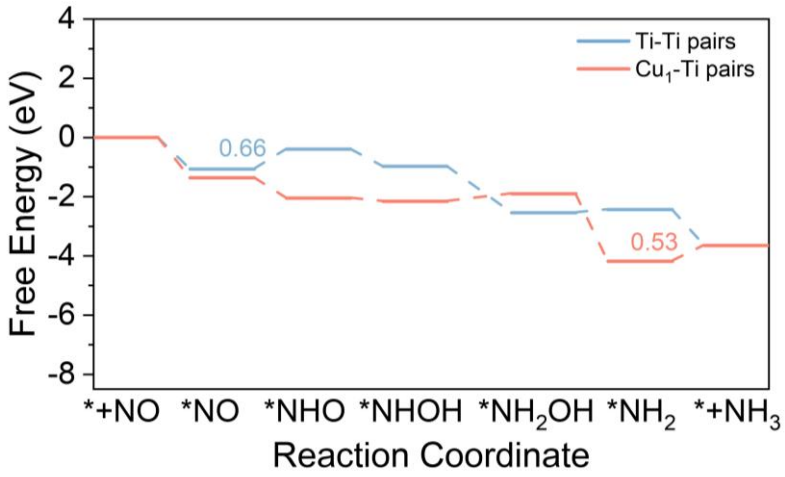

Figure R29. Free energy diagrams for NORR on Ti−Ti pairs and Cu_1−Ti pairs.

7. The introduction barely compares with the latest heteronuclear dual-atom NORR catalysts. Add key performance parameters (FE, yield) of recent works to highlight this study's innovation.

Response: We thank the reviewer very much for these kind comments. As suggested, we have supplemented the NORR performance comparison with the latest heteronuclear dual-atom NORR catalysts, and incorporated key performance parameters (FE; NH_3 yield rate) of recent relevant works to highlight the innovation and advantages of this study.

The related discussion was added on **Page 4 Line 59-63** in the revised manuscript as follows:

"At −0.6 V vs. reversible hydrogen electrode (RHE), Cu_1−Ti pairs achieved a high Faradaic efficiency (FE_{NH3}) of 93.7% and yield rate of 189.9 μmol h^{-1} cm^{-2}, both of which were superior to those of Ti−Ti pairs (63.5%, 58.5 μmol h^{-1} cm^{-2}) and the reported heteronuclear dual-atom NORR catalysts, like CuFe DS/NC (90%, 112.52 μmol h^{-1} cm^{-2}).[31]"

References

1. Yu M, Trinkle DR. Accurate and efficient algorithm for Bader charge integration. *J Chem Phys* **134**, 06411 (2011).
2. Tang W, Sanville E, Henkelman G. A grid-based Bader analysis algorithm without lattice bias. *J Phys Condens Matter* **21**, 084204 (2009).
3. Sanville E, Kenny SD, Smith R, Henkelman G. Improved grid-based algorithm for Bader charge allocation. *J Comput Chem* **28**, 899-908 (2007).
4. Xie LF*, et al.* Modulating the Bader Charge Transfer in Single p-Block Atoms Doped Pd Metallene for Enhanced Oxygen Reduction Electrocatalysis. *Angewandte Chemie-International Edition* **63**, e202407658 (2024).
5. Tang WD*, et al.* Hypo-electronegativity Atoms Induce Bader Charge Enrichment on the Pt Surface to Promote Ampere-Level Electrocatalytic Ammonia Oxidation. *J Phys Chem Lett* **16**, 8234-8244 (2025).
6. Li XD*, et al.* Designing multi-metal-site nanosheet catalysts for CO_2 photoreduction to ethylene. *Nat Commun* **16**, 6500 (2025).

Point-by-point responses to the reviewers' comments

The reviewers' comments are laid out below in *Italic font* and our responses are given in normal font and the changes/additions are highlighted in the revised manuscript with using blue colored text.

Reviewer #1 (Remarks to the Author):

The authors did a lot of work to the comment, which convinced me to change my mind. I can recommend its publication.

Response: We sincerely appreciate your constructive comments, which have greatly enhanced the quality of our work.

Reviewer #2 (Remarks to the Author):

The authors addressed my questions perfectly and I agree it to publish in Nature Communications.

Response: We sincerely appreciate your constructive comments, which have greatly enhanced the quality of our work.

Reviewer #3 (Remarks to the Author):

The authors have well addressed the concerns according to the reviewers' suggestions by providing supporting data and evidence with appropriate discussions, which further enhanced the quality of the manuscript. The reviewer thus suggests the acceptance of the revised manuscript.

Response: We sincerely appreciate your constructive comments, which have greatly enhanced the quality of our work.

Reviewer #4 (Remarks to the Author):

After the revision, the authors have made considerable efforts and devoted substantial length to address the issues we raised with scientific revisions and responses. Characterizations are also comprehensive to help understand this result. Therefore, this manuscript meets the high standards required for publication in the "Nature Communications" after addressing the following concerns.

Attention should be paid to the title. It is evident that this is a heterogeneous catalytic system; however, the title is highly misleading because it strongly suggests a homogeneous one. Therefore, TiOx or other substrates should be essential in this manuscript, including the title, all figures, and figure captions.

Response: We sincerely appreciate your constructive comments, which have greatly enhanced the quality of our work. We recognize the ambiguity of the original title, which may imply a homogeneous catalytic system. Following your suggestion, we have revised the title to "Bidirectional electron donation in Cu_1−Ti pairs on TiO_x for efficient nitric oxide electroreduction". Nevertheless, we found that adding TiO_x to catalyst labels (e.g., Ti−Ti pairs/TiO_x, Cu_1−Ti pairs/TiO_x) in figures and captions would cause confusion. Such notation could be misinterpreted as three active sites, while our system only contains dual paired sites. For this reason, we only incorporated TiO_x into the title to clarify the heterogeneous nature, and did not add it to figure labels and captions.

Reviewer #5 (Remarks to the Author):

The authors have positively responded all the comments raised by the reviewers. Therefore, I recommend the acceptance of this paper for publication.

Response: We sincerely appreciate your constructive comments, which have greatly enhanced the quality of our work.